RSC Advances

PAPER

View Article Online
View Journal | View Issue

Cite this: *RSC Adv.*, 2024, **14**, 1995

New pyrazolo[3,4-*d*]pyrimidine derivatives as EGFR-TK inhibitors: design, green synthesis, potential anti-proliferative activity and P-glycoprotein inhibition†

Aya I. Hassaballah, *[a] Asmaa M. AboulMagd, *[b] Magdy M. Hemdan,[a] Mohamed H. Hekal,[a] Amira A. El-Sayed[a] and Paula S. Farag[a]

Received 9th August 2023
Accepted 22nd December 2023

DOI: 10.1039/d3ra05401b

rsc.li/rsc-advances

In this study, four series of new pyrazolo[3,4-*d*]pyrimidine derivatives were designed and synthesized with both green and conventional methods. All the synthesized candidates were chemically confirmed using spectroscopic methods, and the DFT of the reaction mechanism was illustrated. The anti-proliferative activity of the synthesized compounds was evaluated against NCI 60 cancer cell lines. Two compounds (**15** & **16**) exhibited excellent broad-spectrum cytotoxic activity in NCI 5-log dose assays against the full 60-cell panel with GI_{50} values ranging from 0.018 to 9.98 μM. Moreover, the enzymatic assessment of the most active derivatives **4**, **15**, and **16** against EGFR tyrosine kinase showed significant inhibitory activities with IC_{50} of 0.054, 0.135, and 0.034 μM, respectively. The quantitative real-time PCR for the P-glycoprotein effect of compounds **15** and **16** was examined and illustrated the ability to inhibit the P-glycoprotein by 0.301 and 0.449 fold in comparison to the control. Mechanistic study using reversal activity in MDA-MB-468 cell line revealed the effect of both compounds **15** and **16** cytotoxicity against DOX/MDA-MB-468 with IC_{50} = 0.267 and 0.844 μM, respectively. Additionally, compound **16** was found to induce cell cycle arrest at the S phase with a subsequent increase in pre-G cell population in MDA-MB-468 cell line. It also increased the percentage of apoptotic cells in a time-dependent manner. Moreover, a molecular docking study was carried out to explain the target compounds' potent inhibitory activity within the EGFR binding site.

1. Introduction

Protein Tyrosine Kinases (PTKs) represent a large family of proteins that play a crucial role in many cellular activities including growth, differentiation, metabolism, adhesion, motility, and death.[1–4] Numerous pathological diseases, including cancer are influenced by the aberrant catalytic activity of many PTKs caused by mutation or over-expression.[5–7] The trans-membrane growth factor receptor PTK family includes many members, of these are the epidermal growth factor receptor (EGFR) family. The EGFR family has four members: HER2 (human epidermal growth factor receptor-2; also known as erbB2), HER1 (epidermal growth factor receptor; EGFR), HER3, and HER4. Numerous cancers of epithelial origin, including colon, breast, ovarian, and NSC lung cancer, have been linked to EGFR overexpression.[8] So, to design novel anticancer therapies that work by competing with ATP for binding at the catalytic domain of their target enzyme, EGFR inhibition constitutes a logical strategy.[9] In cancer clinical trials, a variety of small molecule EGFR kinase inhibitors have been evaluated. For instance, erlotinib[10] (**I**) and gefitinib[11] (**II**) are anilinoquinazoline-containing drugs that have been authorized for the chemotherapeutic treatment of individuals with advanced non-small lung cancer. Lapatinib (**III**) was also given the go-ahead to treat breast cancer[12,13] (Fig. 1). Investigation of the clinically used EGFR-TK inhibitors showed that they should possess four pharmacophoric features to bind efficiently within the ATP binding pocket of EGFR-TK.[14,15] The first feature is a flat heteroaromatic ring that can occupy the adenine binding pocket. The second one is a terminal hydrophobic tail to be embedded in the first hydrophobic groove of EGFR. The third pharmacophoric feature is a spacer that can bind *via* hydrogen bond interactions. Finally, one more hydrophobic tail occupies the hydrophobic II region of ATP.

Pyrazolo[3,4-*d*]pyrimidin-4(5*H*)-one is a bioisostere naturally occurring purine nucleoside heterocyclic base that is thought to be a main skeleton in some biologically active compounds. Differently substituted pyrazolo[3,4-*d*]pyrimidin-4(5*H*)-ones

[a]*Chemistry Department, Faculty of Science, Ain Shams University, Abbassia, 11566, Cairo, Egypt. E-mail: ayaibrahim@sci.asu.edu.eg*

[b]*Pharmaceutical Chemistry Department, Faculty of Pharmacy, Nahda University (NUB), Beni-Suef, Egypt. E-mail: asmaa.aboulmaged@nub.edu.eg*

† Electronic supplementary information (ESI) available. See DOI: https://doi.org/10.1039/d3ra05401b

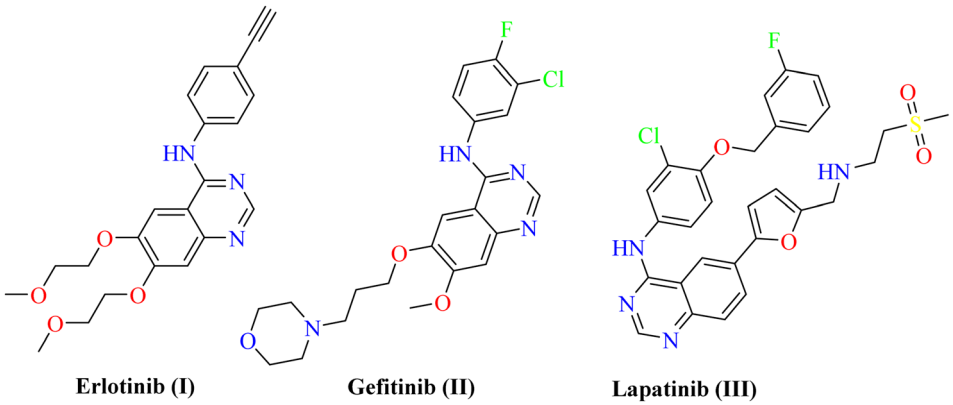

Fig. 1 FDA-approved EGFR-TK inhibitors.

exhibit a wide range of pharmacological properties, including anti-inflammatory,[16] anti-bacterial,[17] anti-fungal,[18] anti-viral,[19] anti-microbial,[20] CNS-modulating,[21] anti-oxidant,[22] and cardiovascular agents.[23] Other pyrazoloprymidinone derivatives are also used to manage type II diabetes[24] and insomnia.[25] Moreover, the pyrazolo[3,4-*d*]pyrimidin-4(5*H*)- derivatives are considered as potential pharmacophores of several analogs that display anti-cancer activity against human colon (HCT-116),[26] human leukemia (HL-60),[27] non-small cell lung cancer (NCL-H 460), CNS cancer (SF- 268),[28] and skin cancer cell lines (G-361).[29] Additionally, hybrid molecules that built up *via* joining more than one pharmacophore are suggested to exhibit better activity than the individual activity of each isolated one. Thus, sunitinib (**IV**) and toceranib (**V**) are indoline-2-one derivatives that have been approved by the US FDA for cancer therapy. Also, compound **VI** was reported as an ATP-competitive inhibitor exerting EGFR inhibitory effect with nanomolar concentration.[30] Compound **VII** is another 1*H*-pyrazolo [3,4-*d*]pyrimidine derivative with significant anti-EGFR activity[31] (Fig. 2). Based on the mentioned evidences considering the potential EGFR as an anticancer target, the resistance arise against the FDA approved anticancer drugs, and the attractiveness of 1*H*-pyrazolo[3,4-*d*] pyrimidine moiety, it was interesting to design and synthesize new 1*H*-pyrazolo[3,4-*d*]pyrimidine derivatives that may exhibit possible anti-proliferative and EGFR inhibitory activity. Accordingly, the synthesized compounds were designed to have the essential pharmacophoric features of EGFR inhibitors.

1.1. Rational of the work

Based on the previous results, regarding the potential anticancer activity of pyrazolo[3,4-*d*]pyrimidines, we herein, report the design and synthesis of a new series of pyrazolo [3,4-*d*]pyrimidine derivatives to evaluate their possible anti-proliferative activity and EGFR-TK inhibitory activity. In this work, 1*H*-pyrazolo[3,4-*d*]pyrimidine moiety was used as a heteroaromatic ring system occupying the adenine binding region.[32,33] Also, phenyl ring was utilized as a hydrophobic moiety to occupy the hydrophobic region I of the ATP-binding site. The linker was reserved to make the essential binding interactions. Different moieties include

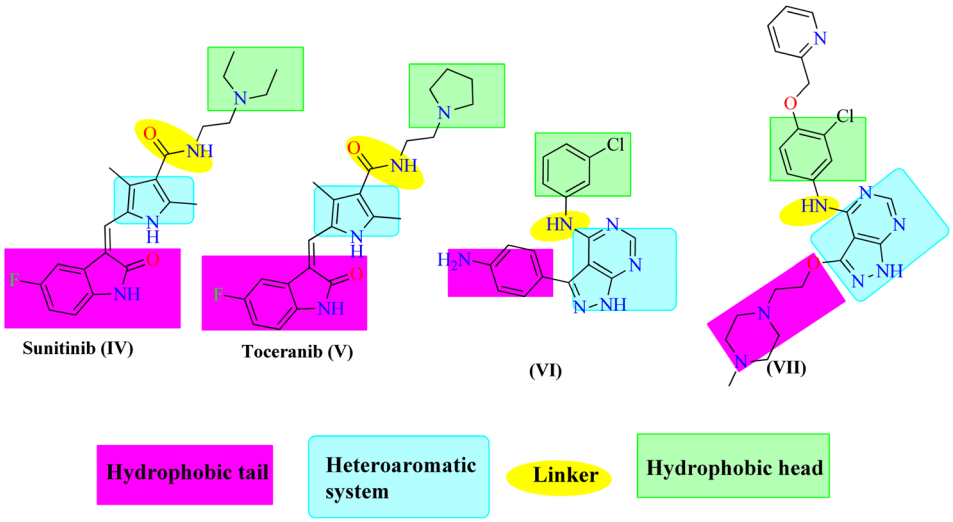

Fig. 2 EGFR inhibitors and their pharmacophoric features.

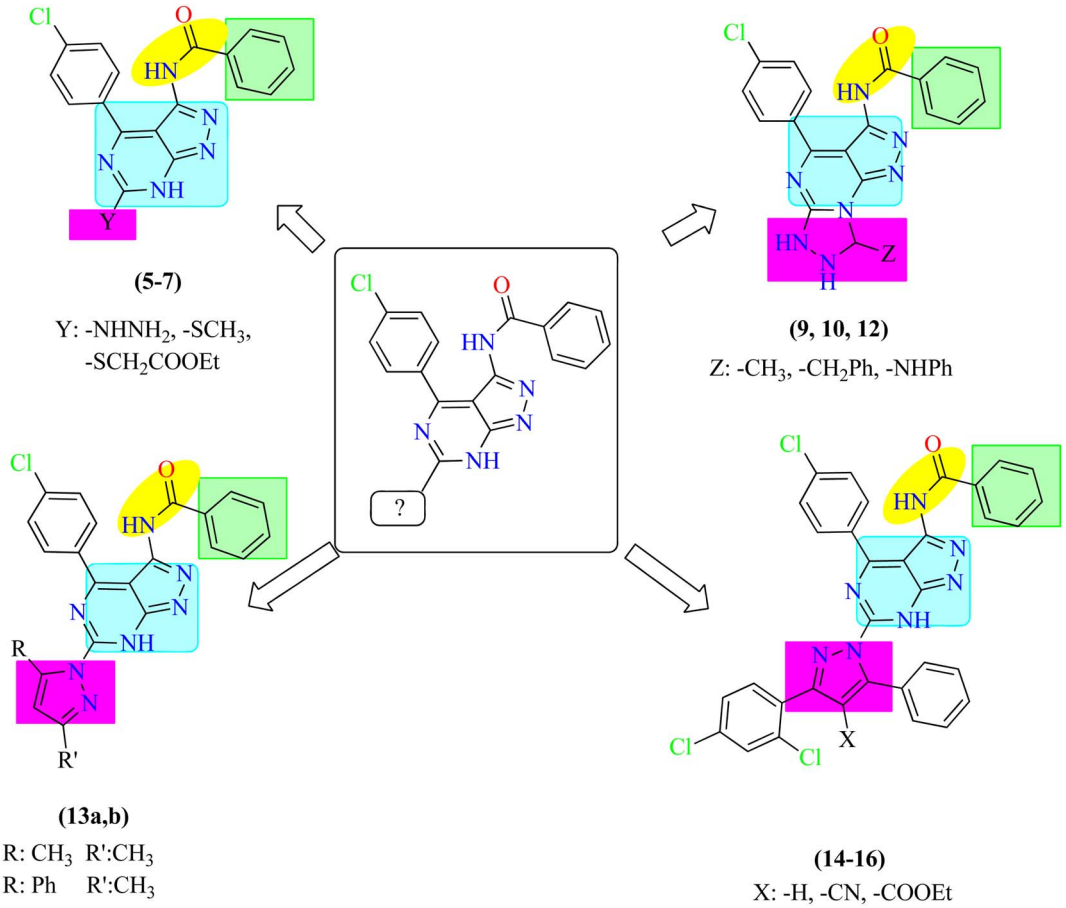

Fig. 3 Rationale of molecular design of the new proposed EGFR-TK inhibitors.

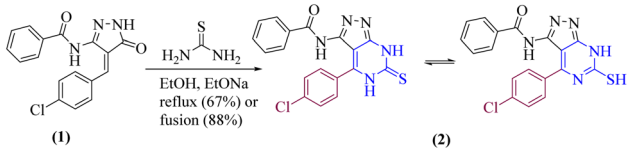

Scheme 1 Synthesis of pyrimidinthione derivatives 2 under both conventional and green conditions.

substituted phenyl ring, tricyclic rings and aliphatic substituents were used to occupy the hydrophobic region II of the ATP-binding site to discover their possible cytotoxic activity. Correlation between the structure–activity relationship of the synthesized compounds and their antiproliferative activity targeting EGFR was discussed due to these modifications (Fig. 3).

2. Results and discussion

2.1. Chemistry

Our current research is concerned with the utility of *N*-(4-(4-chlorobenzylidene)-4*H*-pyrazol-3-yl)benzamide **(1)** in the synthesis of new substituted fused pyrimidine derivatives under conventional and green conditions as part of our interest in the synthesis of a wide range of heterocyclic systems with biological applications.[34–37]

The starting chemical, *N*-(4-(4-chlorobenzylidene)-5-oxo-4,5-dihydro-1*H*-pyrazol-3-yl)benzamide **(1)**, was synthesized according to an earlier reported procedure[38] under different chemical reaction conditions. Thus, refluxing of compound **1** with ethanolic solution of thiourea in the presence of catalytic amount of sodium ethoxide or under free solvent fusion technique to afford the target compound *N*-(4-(4-chlorophenyl)-6-thioxo-6,7-dihydro-5*H*-pyrazolo[3,4-*d*]pyrimidin-3-yl)benzamide **(2)** with a beneficial yield, which was used as a key starting material as illustrated in (Scheme 1).

The structure of compound **2** was determined using spectroscopic data. Their IR spectra showed absorption bands corresponding to the –NH and –C=O groups at υ 3197 br and 1681 cm^{-1}, respectively as well as the presence of –NH groups at υ 11.46, 11.86 and 12.40 ppm in the ^{1}H-NMR spectrum of compound **2** which agree well with the suggested structure.

Moreover, we illustrate the reaction of a secondary amine in absolute ethanol with the presence of a basic medium and a nitrosating agent. It was crucial to emphasize that, in these conditions, the absence of acidic conditions mitigates the risk of *N*-nitrosamine formation.[39,40]

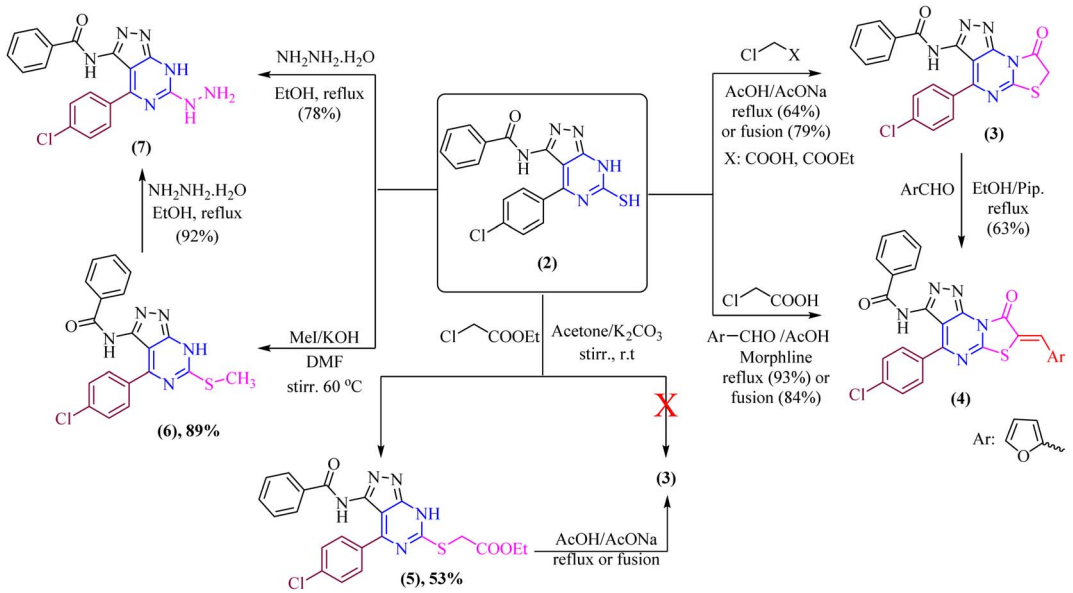

Scheme 2 Reaction of thiol derivative **2** with different electrophiles and nucleophiles.

The di-heterocyclic compound **2** was established and used as a mediator to synthesize tri-heterocyclic compounds linked with pyrazolopyrimidine moiety. Thus, refluxing of thiol derivative **2** with chloroacetic acid and/or ethyl chloroacetate in glacial acetic acid with sodium acetate anhydrous afforded thiazolo[3,2-*a*]pyrimidine derivative **3** as the sole product as shown in (Scheme 2). Compound **3** was also obtained by free solvent fusion condition for 75 min. Treatment of thiazolo[3,2-*a*]pyrimidine derivative, compound **3**, with 2-furancarboxaldehyde yielded the corresponding condensation product, which surprisingly *in situ* undergoes knoevenagel condensation by presence of piperidine catalyst to give *N*-(4-(4-chlorophenyl)-7-(furan-2-ylmethylene)-8-oxo-7,8-dihydropyrazolo[4,3-e]thiazolo[3,2-*a*]pyrimidin-3-yl)benzamide, compound **4** as the sole product (one spot in TLC), which also obtained by fusion technique under solvent-free condition (Scheme 2). Likewise, compound **4** was obtained *via* one-pot multicomponent condensation reactions of **2**, chloroacetic acid, and furfural, with morphline as a catalytic base to afford the corresponding thiazolo[3,2-*a*]pyrimidine derivative **4**.

On another hand, by stirring of thiol derivative **2** at room temperature with ethyl chloroacetate in the presence of a catalytic amount of anhydrous potassium carbonate in dry acetone afforded uncyclized *S*-alkylated product ethyl 2-((3-benzamido-4-(4-chlorophenyl)-7*H*-pyrazolo[3,4-*d*]pyrimidin-6-yl)thio) acetate (**5**) as demonstrated in (Scheme 2) with no evidence was verified for the cyclized structure **3**. Likewise, cyclization of *S*-alkylated product **5** *via* one-pot multicomponent condensation reactions of **5** with acetic acid in the presence of sodium acetate afforded the corresponding thiazolo[3,2-*a*]pyrimidine derivative **3** as the sole product. The absorption bands for the –CO ester group at υ 1717 cm^{-1} in the IR spectra verified the uncyclized *S*-alkylation. Furthermore, the ^{1}H-NMR spectrum of compound **5** revealed the presence of a triplet at δ 2.06 ppm and a quartet at δ 4.35 ppm with equal coupling constants typical of $-CH_2CH_3$ protons, as well as a singlet signal at 5.44 ppm for $-CH_2-$ COOEt protons, all of which are completely consistent with the uncyclized structure, compound **5** with ruling out the cyclized product **3**. Furthermore, the ^{13}C-NMR spectrum of structure **5** matches the hypothesized structure well.

Moreover, methylthio derivative **6** was produced in 89% yield when thiol derivative **2** was alkylated by methyl iodide in dry *N*,*N*-dimethylformamide and in the presence of potassium hydroxide was stirred at 60 °C for 2.5 hours. The spectral data and the elemental analyses of the synthesized compound **6** were in accordance with the proposed structures of compound **6** (Scheme 2). The ^{1}H-NMR spectrum showed the signal of the $-CH_3$ group at δ 3.57 ppm. In addition, ^{13}C-NMR spectra were consistent with the proposed structure.

Furthermore, the refluxing of ethanolic solution of thiol derivative **2** with hydrazine hydrate afforded hydrazineyl-7*H*-pyrazolo[3,4-*d*]pyrimidin derivative **7**. Additionally, hydrazinolysis of the methylthio derivative **6** with a molar ratio [1 : 1] in absolute ethanol was heated under refluxing (one spot in TLC) (Scheme 2). The IR spectrum of compound **7** showed the appearance of –NH and $-NH_2$ groups at υ 3424, 3309, and 3224 cm^{-1}, respectively. Additionally, the structure of compound **7** is supported by the ^{1}H-NMR spectrum [DMSO-d_6], which exhibited signals for $-NH_2$ group at δ 7.27 ppm as well as –NH protons in the downfield region that might be exchanged with D_2O. Furthermore, the ^{13}C-NMR spectrum of structure **7** matches the hypothesized structure well.

Chemical cyclization of hydrazine derivative **7** into distinct heterocyclic compounds having fused pyrazolo[3,4-*d*]pyrimidin scaffold has been explored under various chemical reaction circumstances, as shown in (Scheme 3). Thus, heating of compound **7** in water-bath with carbon disulfide in dry pyridine afforded thioxo-pyrazolo[4,3-*e*][1,2,4]triazolo[4,3-*a*]pyrimidin

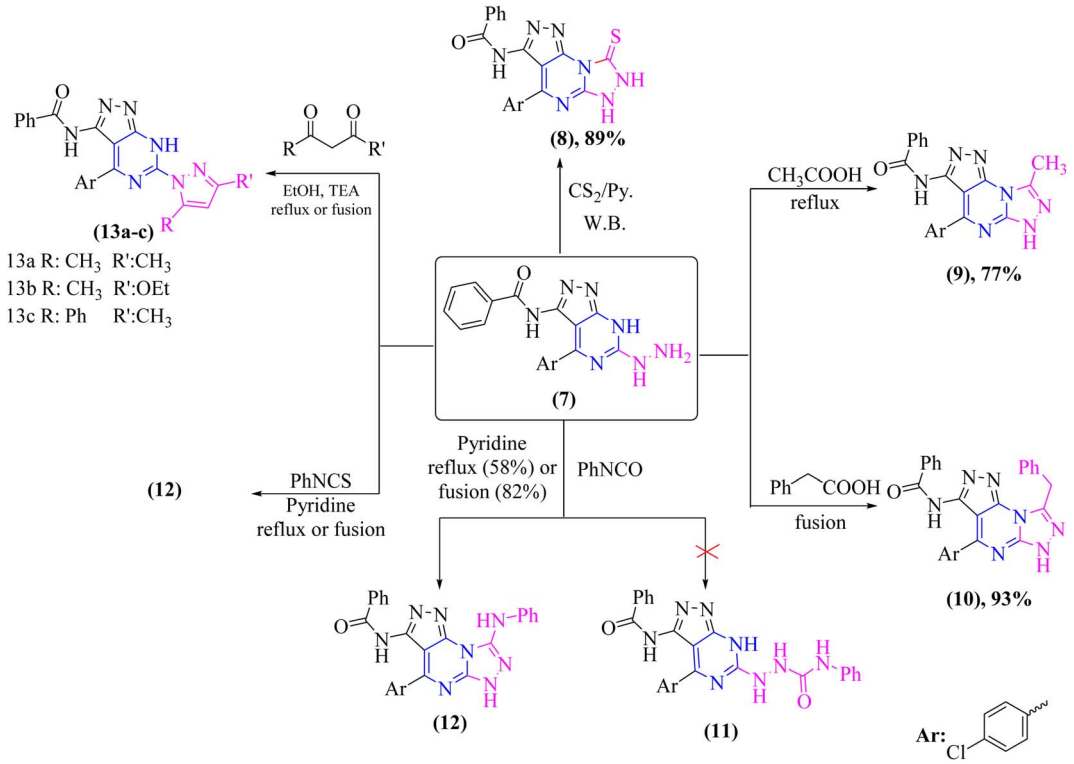

Scheme 3 Cyclization of hydrazine derivative 7 to afford fused tri-heterocyclic compounds.

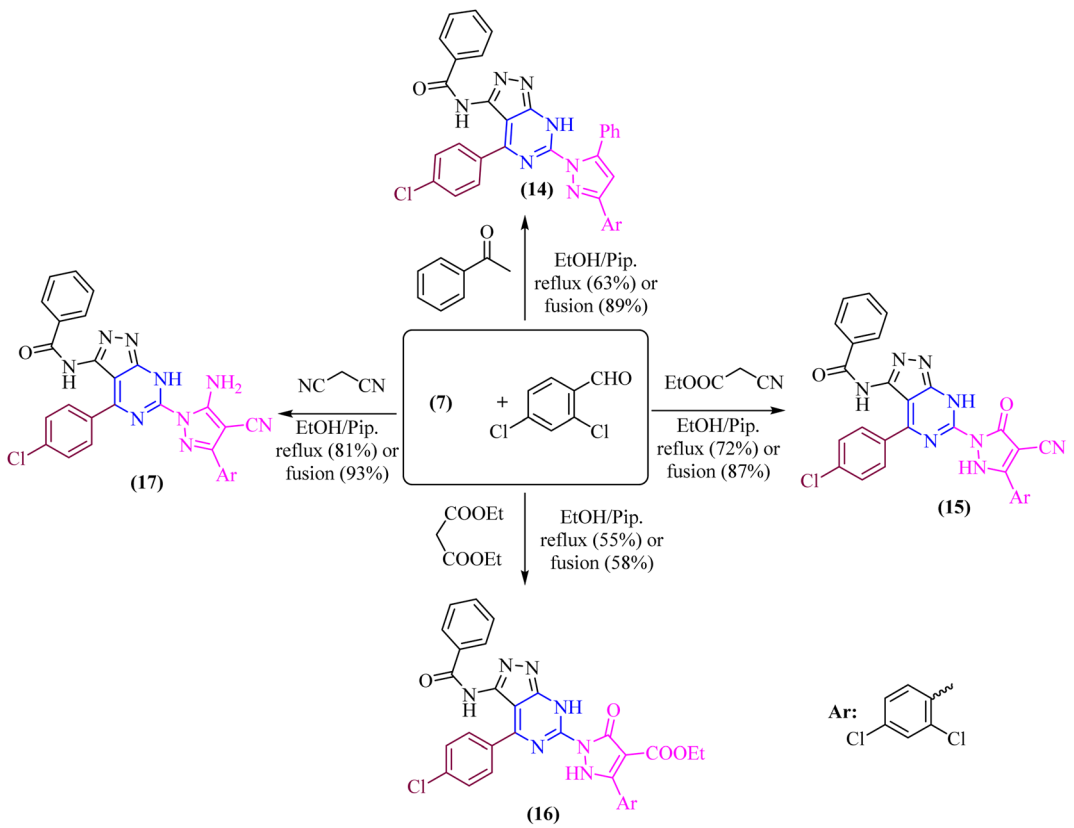

Scheme 4 One-pot multicomponent condensation reactions 7, and 2,4-dichlorobenzaldehyde with different active methylene.

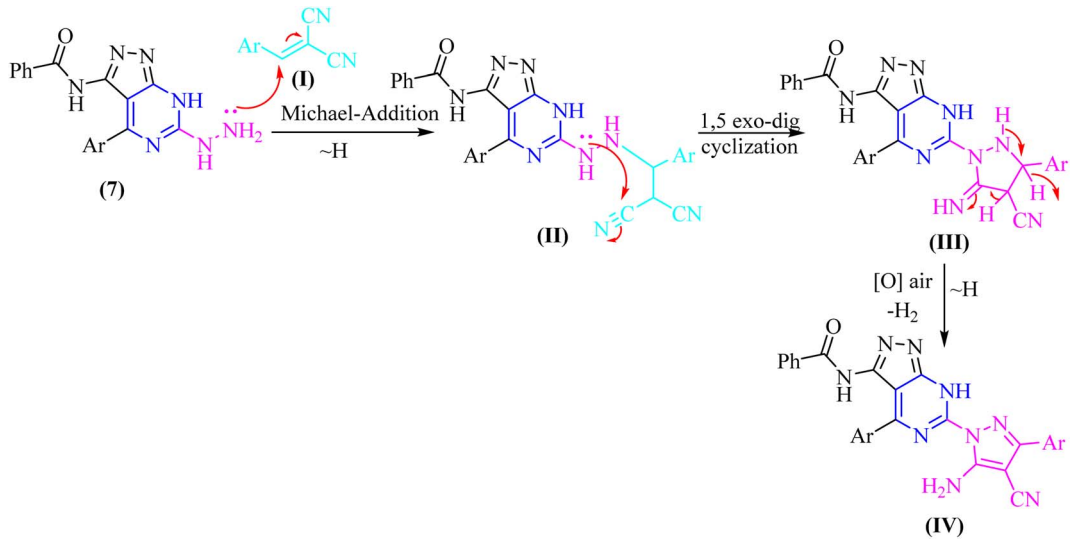

Scheme 5 Suggested mechanism for the formation of compounds **14–17**.

derivative, compound **8** in a rationally good yield (89%). Compound **8** lacked in its IR spectrum, the strong absorption band for –NH groups at υ 3180 and 3164 cm^{-1} with disappearing $-NH_2$ group of compound 7. Furthermore, ^{1}H-NMR spectrum of compound **8** displayed D_2O exchangeable protons of –NH groups at δ 8.25, 11.44, and 13.39 ppm. In addition, the ^{13}C-NMR spectrum of structure **8** agrees with the hypothesized structure well.

In addition, refluxing of compound 7 in glacial acetic acid for 3 h afforded *N*-(4-(4-chlorophenyl)-8-methyl-6*H*-pyrazolo[4,3-*e*][1,2,4]triazolo[4,3-*a*]pyrimidin-3-yl)benzamide **(9)** (Scheme 3). Moreover, compound 7 was fused under solvent-free condition with phenyl acetic acid afforded pyrazolo[4,3-*e*][1,2,4]triazolo[4,3-*a*]pyrimidin derivative **10** as the sole product in a good yield (93%). The proper elemental analysis and spectroscopic data provided sufficient proof for the chemical structure of compounds **9** and **10**. Both compounds' ^{1}H-NMR spectra [DMSO-d_6] revealed signals corresponding to methyl and methylene protons of **9** and **10**, respectively, and –NH protons in the down field area that could be exchanged with D_2O. Furthermore, the ^{13}C-NMR spectra of structures **9** and **10** revealed signals that matched the hypothesized structure (*cf.* experimental).

Moreover, treatment of hydrazine derivative 7 with phenyl isocyanate in refluxing pyridine for 15 hours yielded the unexpected pyrazolo[4,3-*e*][1,2,4]triazolo[4,3-*a*]pyrimidine derivative

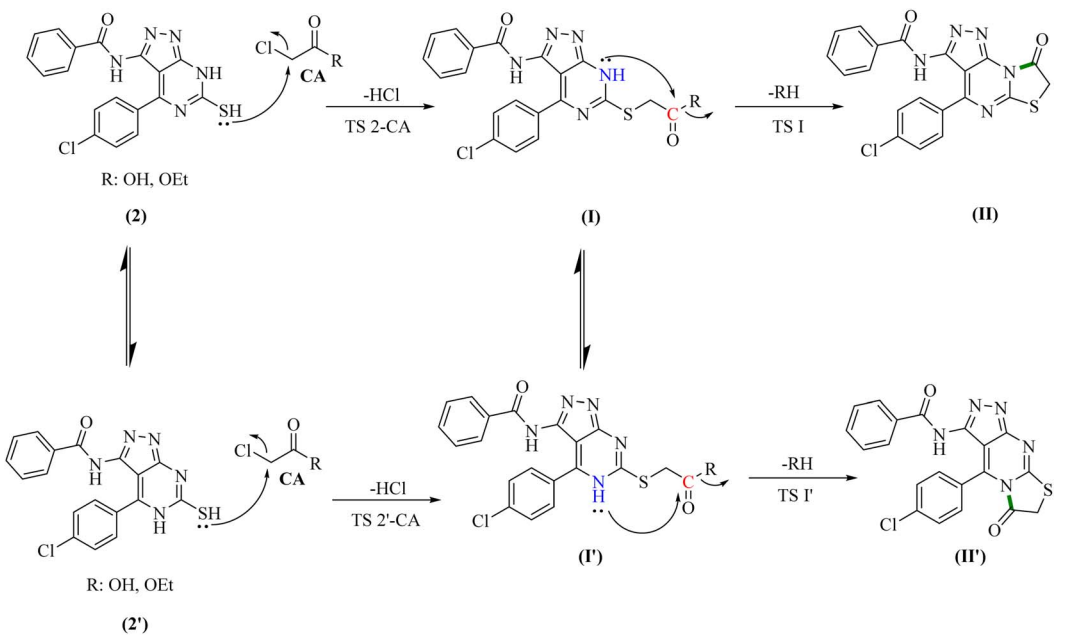

Fig. 4 Two proposed reaction pathways of for the first reaction.

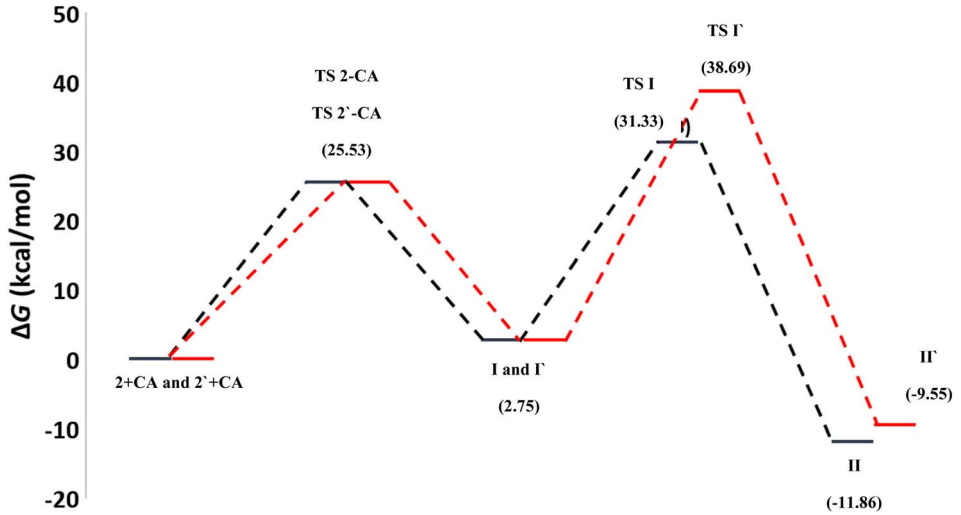

Fig. 5 Potential energy curves for the reaction pathways of the first reaction.

11 rather than the uncyclized *N*-phenylhydrazine-1-carboxamide derivative **12** as illustrated in (Scheme 3).

Furthermore, refluxing compound 7 with phenyl isothiocyanate in dry pyridine for 15 hours or fusing it under free solvent condition for 2 hours afforded a sulfur-free product known as *N*-(4-(4-chlorophenyl)-8-(phenylamino)-6*H*-pyrazolo[4,3-*e*][1,2,4]triazolo[4,3-*a*]pyrimidin-3-yl)benzamide **(12)** (Scheme 3). The proper elemental analysis and spectroscopic data provided sufficient proof for the chemical structure of compound **12**.

The fused di-heterocyclic compound 7 was employed as a starting material to synthesize tri-heterocyclic compounds with attached the pyrazolopyrimidine moiety. As indicated in (Scheme 3), treatment of compound 7 under both conventional and solvent free fusion conditions with different diketone derivatives such as acetyl acetone, ethyl acetoacetate, and/or benzoyl acetone yielded (pyrazol-1-yl)-7*H*-pyrazolo[3,4-*d*]pyrimidin derivatives **13a–c**. The elemental analysis and spectral data IR and NMR of the produced compounds were compatible with the predicted structures of compounds **13a–c**. The IR spectrum of compounds **13a–c** revealed the elimination of the $-NH_2$ group. Moreover, the ^{1}H-NMR and ^{13}C-NMR spectra were in concurrence with the proposed structures **13a–c**.

In both techniques, conventional and green conditions, one-pot multicomponent reactions of 7, and 2,4-dichlorobenzaldehyde in the presence of acetophenone, ethyl cyanoacetate, diethyl malonate, and/or malononitrile yielded the corresponding (1*H*-pyrazol-1-yl)-4-(4-chlorophenyl)-7*H*-pyrazolo[3,4-*d*]pyrimidin derivatives **14–17** as shown in (Scheme 4). The reaction mixture is refluxed or fused under solvent free conditions in absolute ethanol with a catalytic quantity of piperidine to produce arylidene derivatives **(I)** *in situ* as illustrated in (Scheme 5), resulting in Michael adducts that undergo intramolecular cyclization **(II)** to give the target derivatives **14–17** as the suggested mechanism (Scheme 5).

Microanalytical and spectral data corroborated the structure of compounds **14–17**. The IR spectra of compound **14** exhibit absorption at υ 3177 and 3062 cm^{-1}, corresponding to the –NH and phenyl groups, respectively. The ^{1}H-NMR spectra of these compounds indicate the phenyl and aromatic protons, in

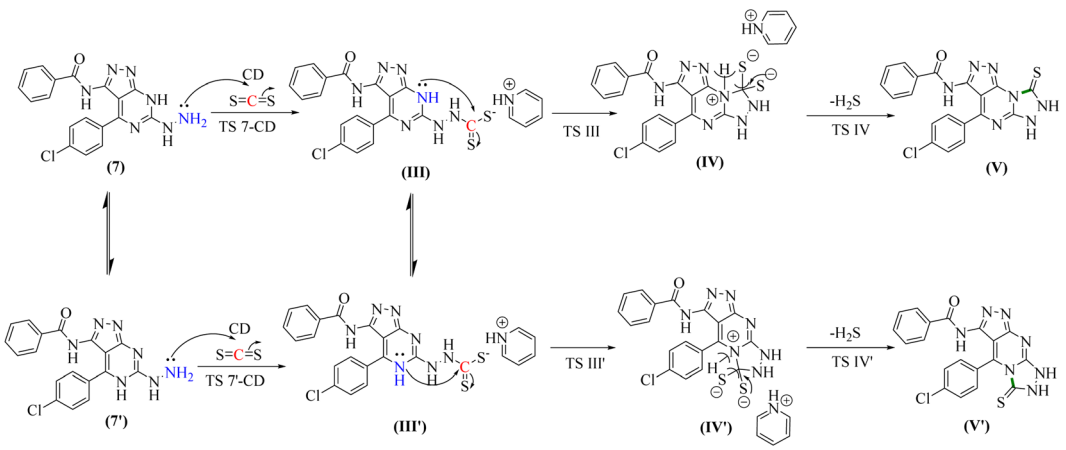

Fig. 6 Two proposed reaction pathways for the second reaction.

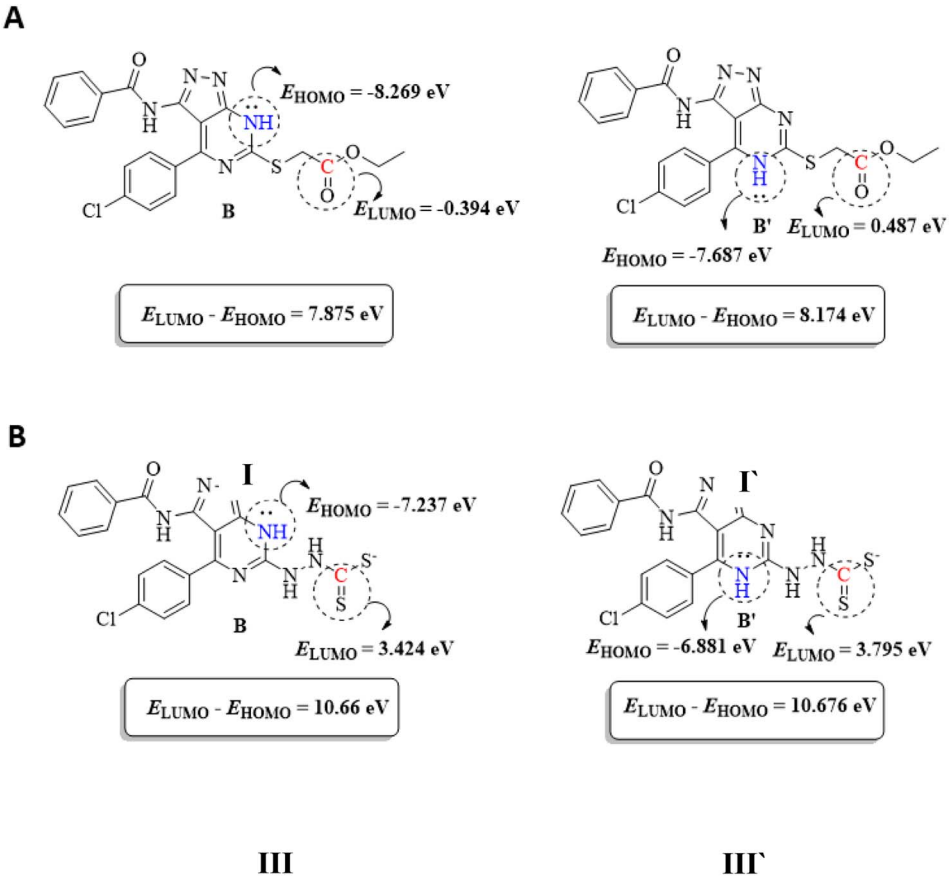

Fig. 7 FMOs of B and B′ for the first and second reactions (A and B, respectively).

addition to the strongly deshielded exchangeable –NH proton at δ 14.14 ppm.

Moreover, the IR spectra of compounds **15** and **16** reveal absorption at υ 2215 and 1715 cm^{-1}, which corresponds to the –CN and –C═O ester groups of **15** and **16**, respectively. The ^{1}H-NMR spectrum of these compounds also exhibits the strongly deshielded exchangeable –NH protons at δ 13.37 and 14.18 ppm of **15** and **16**, respectively as well as the aliphatic protons of –C_2H_5 of compound **16**.

Furthermore, the IR spectrum revealed absorption bands in the range of υ 3210 and 3149 cm^{-1} for –NH_2 and –NH, respectively, and absorption band at υ 2222 and 1657 cm^{-1} for –CN and amidic –CO groups, respectively. The exchangeable wide signals of –NH_2 and amidic –NH in compound **17**, and the aromatic protons in the expected region, were all visible in the ^{1}H-NMR spectrum. Singlet signals were seen in the ^{13}C-NMR spectrum for the C═O, C═N, and C═C groups of compound **17**.

2.2. DFT study of the reaction mechanism

To gain further insight into the reaction mechanisms and their possible pathways, theoretical calculations were carried out using compounds **I** and **I′** as the model reactants (Fig. 1).

First, DFT calculations suggested that the reactants **2** or its tautomer **2′** and **CA** can be converted into I or its tautomer I′ *via* the transition state 2-CA or 2′-CA with an activation energy of 25.53 kcal mol^{-1} (Fig. 4 and 5). At this point of the reaction, I or I′ exhibited intramolecular nucleophilic–electrophilic reaction between one of the –NH and –C═O groups to form either **II** or **II′** accordingly. Transition state **TS I** is more energetically favored than the competing **TS I′** transition states by 7.36 kcal mol^{-1}. In addition, the ΔG of the final step afforded **II** was lower than that afforded **II′** by 2.13 kcal mol^{-1} (Fig. 5). Hence, the formation of **II** is significantly more preferred than **II′**.

The second reaction showed, to some extent, similar findings, where DFT calculations showed that the reactants 7 or its tautomer 7′ and CD formed the intermediate **III** or its tautomer **III′** *via* the transition state (**7-CA** and **7′-CA**, respectively) with an activation energy of 42.58 kcal mol^{-1} (Fig. 6). At this stage of the reaction, **III** or **III′** went into an intramolecular nucleophilic–electrophilic reaction between one of the –NH and –C═S groups to form either **IV** or **IV′** as unstable intermediates. Transition state TS **III** is very slightly energetically favored over TS **III′** transition states by only 0.64 kcal mol^{-1}. Finally, both **IV** and **IV′** afforded D and D′, respectively *via* the transition states TS C and TS C′ with convergent ΔG values of −10.36 and −10.18 kcal mol^{-1}, respectively, and hence, the formation of the final products **V** and **V′** can occur with a slight preference to **V**.

To support the previous findings from the frontier molecular orbital (FMO) perspective, we calculated the LUMO–HUMO energy gap for **I** and **I′** in each reaction. **I** and **I′** are the key

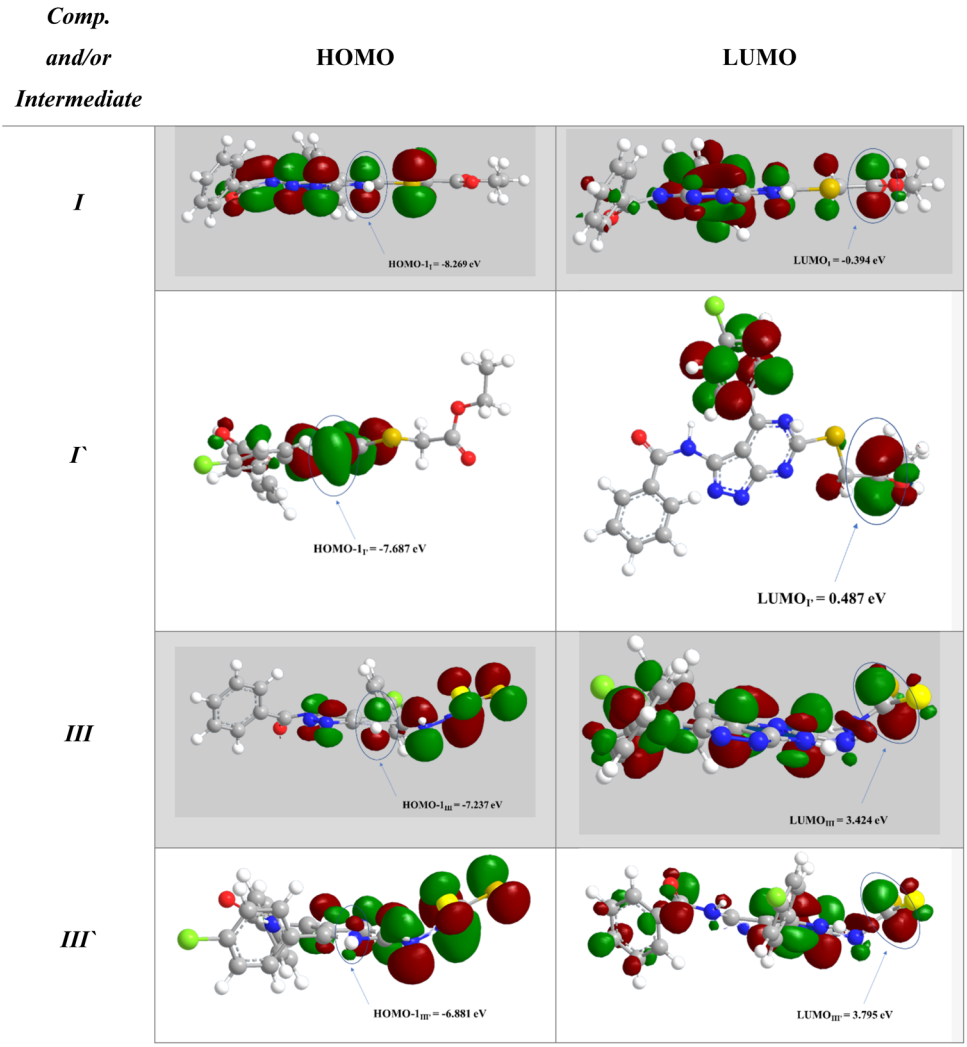

Fig. 8 The frontier molecular orbital (FMO) of HOMO–LUMO.

intermediates in each reaction determining which final product will be formed.

The reacting orbital of the –NH is HOMO-1, while of the –C═O or –C═S group it is LUMO (Fig. 8). In the first reaction, the energy gap between the LUMO and HOMO-1 is 7.875 eV for **I**, while for **I′**, the corresponding energy gap between the two reacting orbitals is 8.174 eV, which is 0.299 eV larger than that in **I**. Therefore, the formation of **II** becomes favored over **II′** (Fig. 7A).

In the second reaction, the LUMO–HOMO-1 energy gap is 10.66 eV for **III**, while it is 10.676 eV for **III′**. Hence, the reaction is slightly favored toward the **III** formation over **III′** formation (Fig. 7B).

Table 1 The EGFR inhibitory activity of compounds **4**, **15** and **16**

Cpd no.	EGFR ± SD IC_{50} (μM)
4	0.054 ± 0.003
15	0.135 ± 0.006
16	0.034 ± 0.002
Lapatinib	0.074 ± 0.003

2.3. Biological activity

2.3.1. Results of *in vitro* primary single dose (10 μM) full NCI 60 cell panel assay. Primary *in vitro* one-dose antiproliferative activity was carried out in a full NCI 60-cell panel. All results were represented as a mean graph of the percent growth of the treated cells when compared to the untreated control cells. Primary *in vitro* single dose anticancer assay was performed in a full NCI 60-cell panel. Results for each compound were reported as a mean graph of the percent growth of the treated cells compared to the untreated control cells. Two of the investigated substituted pyrazolo[3,4-*d*]pyrimidine derivatives showed a distinctive pattern of sensitivity against different NCI cell lines and were chosen for 5 log doses (Tables S1 and S2†). The cyano pyrazole derivative (**15**) linked to pyrazolo[3,4-*d*]pyrimidine moiety exhibited remarkable broad spectrum cell growth inhibition above 90% against various cell lines including leukemia, non-small cell lung cancer, colon, and prostate cancer cell lines. Moreover, it showed highly potent and broad inhibition above 100% against some of the tested melanoma cell lines, ovarian, renal and breast cancer cell lines.

Table 2 The P-glycoprotein inhibitory activity of compounds **15** and **16**

Cpd no.	MDA-MB-468 P-glycoprotein fold change
15	0.301
16	0.449
Control	1

Table 3 Cytotoxic activity of the most active compounds against DOX/MDA-MB-468 cell lines

Cpd no.	DOX/MDA-MB-468 (μM)	±SD
15	0.267	0.001
16	0.844	0.003

Thus, compound (**15**) was selected for five log dose with GI_{50} = 1.18 to 8.44 μM. Also, the ethyl ester analogue (**16**) having ethyl ester substituent at 4-imidazole ring linked to the pyrazolo[3,4-*d*]pyrimidine core revealed significant broad-spectrum cell growth inhibition above 100% against different cell lines including non-small cell lung cancer, colon, CNS, prostate, ovarian, renal cancer and breast cancer cell lines. Interestingly, this analog exhibited spectrum inhibition above 90% against leukemia, NCI-H460 (non – small cell lung cancer cell line), KM12 (colon cancer cell line), U251 (CNS cancer cell line), 786-0 (renal cancer cell line), and breast cancer cell lines. According to the potency of this derivative, it was selected for five log dose with GI_{50} ranges from 0.018 to 9.98 μM.

Also, compound (**4**) showed moderate cell growth inhibition activity among most of the cancer cell lines. Surprisingly, candidate (**6**) revealed poor antiproliferative activity except on HOP-92 which revealed over 100% growth inhibition which may contribute to possible selectivity on HOP-92 (non – small cell lung cancer cell line).

Study of the SAR of the new derivatives showed certain findings. The presence of substituted imidazole ring occupying the hydrophobic pocket II remarkably increases the anticancer activity. Accordingly, compounds **15** and **16**, have the most cytotoxic activity than other analogs either with tricyclic rings or aliphatic tail. This result is consistent with the significance of a terminal hydrophobic ring for the effectiveness of EGFR TK anticancer drugs, previously described. Also, the substitution with a phenyl ring in the tricyclic analog **4** contributes to its moderate cytotoxic activity. Conversely, the presence of tricyclic rings or aliphatic tails showed weak cytotoxic activity.

2.3.2. *In vitro* EGFR tyrosine kinase inhibitory activity. Promising candidates, which exhibited potent antiproliferative activity (**4**, **15** and **16**), were further evaluated for their dose-related EGFR-2 enzymatic inhibition to calculate their IC_{50} values (Table 1). The cyano derivative (**15**) exhibited highly potent EGFR inhibition (IC_{50} of 0.135 μM). Similarly, its analog (**16**) showed significant EGFR inhibitory activity with IC_{50} of 0.034 μM. As for compound (**4**), it revealed a high EGFR inhibitory activity with IC_{50} of 0.054 μM. Investigating the results of EGFR inhibitory activity among the newly synthesized, it was revealed that the results is coherent with the anti-proliferative activity that showed the substitution with imidazole ring increases the EGFR inhibitory activity. It can be observed that the three above mentioned compounds **4**, **15** and **16** shared the presence of imidazole fragment substituited with hydrophilic carbonyl that seems to be important for anticancer activity. Accordingly, compounds **4**, **15** and **16**, incorporating such a fragment, are more strongly cytotoxic than their analogues **17** possessing the same aryl fragment but substituted with an amine group. This finding is in line with the reported significance of the presence of a terminal hydrophobic ring for the potency of EGFR-TK anticancer agents. So, it is noticeable that the three candidates shared the pyrazolo[3,4-*d*]pyrimidine moiety, the aryl ring linker and the substituted phenyl rings that occupied hydrophobic tail and head, forming additional hydrophobic interactions.

2.3.3. Real time PCR for P-glycoprotein. Many mechanisms are involved in cancer multi-drug resistance, the most important one is ATP binding cassette (ABC) protein transporters, especially permeation protein (P-glycoprotein [P-gp]). A quantitative real-time PCR was performed to evaluate the effect of compounds **15** and **16** on P-gp in MDA-MB-468/ADR cells (72 h). The results presented in Table 2 showed that both compounds caused dose-dependent effect on P-gp, where the cyano pyrazole derivative **15** showed a significant inhibitory effect and down-regulation of P-glycoprotein by 0.301-fold in comparison to the control. As for derivative **16**, it showed 0.449 folds inhibition for P-glycoprotein compared to the reference.

2.3.4. *In vitro* cytotoxicity of target compounds 15 and 16 in drug-resistant DOX/MDA-MB-468 cell lines. *In vitro* cytotoxicity of target compounds **15** and **16** in drug-resistant DOX/MDA-MB-468 cells was evaluated. The active anti-proliferative target compound **15** was investigated for its reversal doxorubicin (DOX) effect with IC_{50} = 0.267 μM, Table 3. Additionally, its analogue exhibited IC_{50} = 0.844 μM showing the abilities of both derivatives to be promising candidates in multi-drug resistance.

2.3.5. Cell cycle analysis. EGFR enzyme has been extensively studied to regulate all cell cycle phases.[41] It is a core cell-cycle regulator that is active from the late G_1 phase and throughout the S phase. Thus, it was interesting to gain deep into the mechanism of the potent EGFR inhibitory activity of compound **16** that pointed to its significant antiproliferative activity towards breast cancer cell line MDA-MB-468 as a common susceptible cell line. Therefore, cell cycle analysis was performed to explore the mechanistic action for compound **16**. The results revealed that the accumulation of cells in the G_1 phase of the cell cycle (57.41%) compared to the control, which showed only 52.76% accumulation. Also, there is an increase in the S phase with 28.16% compared to control 22.98%. Thus, it can be concluded that the increase in the proportion of cell cycle arrest for compound **16** resulted in G_1 and S phases arrest pattern through inhibition of EGFR enzyme (Fig. 9).

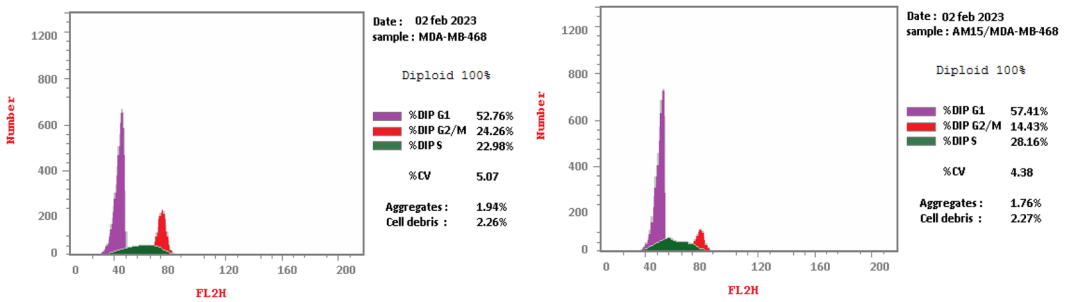

Fig. 9 Flow cytometric analysis of cell cycle phases after treatment with compound **16**.

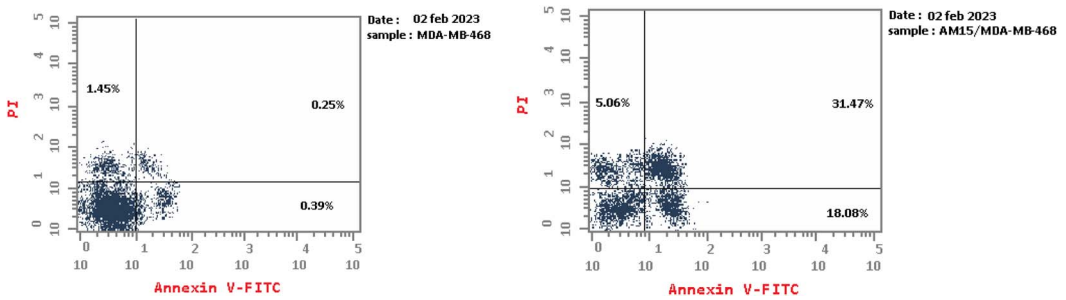

Fig. 10 Flow cytometric analysis of apoptosis in MDA-MB-468 cells exposed to compound **16**.

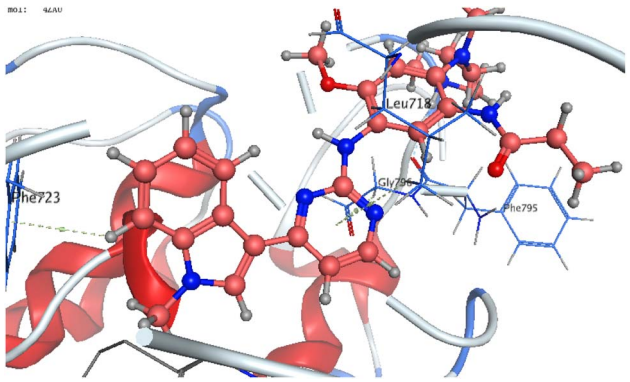

Fig. 11 Three-dimensional binding modes of YY3 inside the binding pocket of EGFR-TK.

2.3.6. Apoptosis assessment. Apoptosis is integral in eliminating neoplastic cells and is thus regarded as a preventive mechanism against cancer growth. A hallmark of cancer is the ability of malignant cells to evade apoptosis, with forthcoming novel anticancer agents demonstrating their effectiveness by triggering the apoptotic process by stimulating proapoptotic molecules and inhibiting anti-apoptotic ones. Flow cytometry was used in MDA-MB-468 cells to evaluate the induction of apoptosis using propidium iodide (PI) and annexin-V-FITC. After post-treatment with IC_{50} of compound **16**, the results illustrate a marginal increase of total apoptosis from 2.09% (DMSO control) to 46.59%, with an increase in the late cellular apoptosis from 0.27% (DMSO control) to 54.61% was observed. Also, there was an increase in early/primary apoptosis from 0.39% (DMSO control) to 18.08% and in the late apoptosis from 0.25% to 31.47% (Fig. 10). These results indicate that the tested compounds significantly promote apoptosis of cancer cells.

2.3.7. Molecular modeling studies. Using MOE 2022.02 software, *in silico* molecular docking simulations were further carried out for the most active compounds **4**, **15** and **16** to support the biological results and predict their preferred binding modes in EGFR enzyme. The docking study was validated by re-docking the co-crystalized ligand YY3 inside the EGFR kinase active site (PDB ID: 4ZAU), and the calculated root-mean-square deviation (RMSD) between the co-crystalized ligand and the docked pose was 1.87 Å.

The co-crystallized ligand of EGF showed a binding score of -7.03 kcal mol^{-1} and its binding mode was represented in Fig. 11. The heterocyclic pyrimidine moiety was oriented into the adenine pocket forming two hydrophobic interactions with Gly796, and Leu718. The phenyl moiety occupied the hydrophobic pocket I forming one hydrophobic interactions with Phe723. The terminal amine forms a hydrogen bond donor interaction with Phe795. Taking candidate **15** as one of the most active cytotoxic compounds, it showed a similar binding pattern to the ligand. Compound **15** displayed a binding score of -7.410 kcal mol^{-1}. The 1*H*-pyrazolo[3,4-*d*]pyrimidin- 6-amine moiety oriented into the adenine pocket to form one hydrogen bond interaction with Met793. Also, it formed one hydrophobic interaction with Gly796. The dichlorophenyl moiety occupied the hydrophobic tail forming one hydrophobic interaction with Lys728. The phenyl ring connected to the amide linker occupied the hydrophobic head forming one hydrophobic interactions with Lys745, Fig. 12.

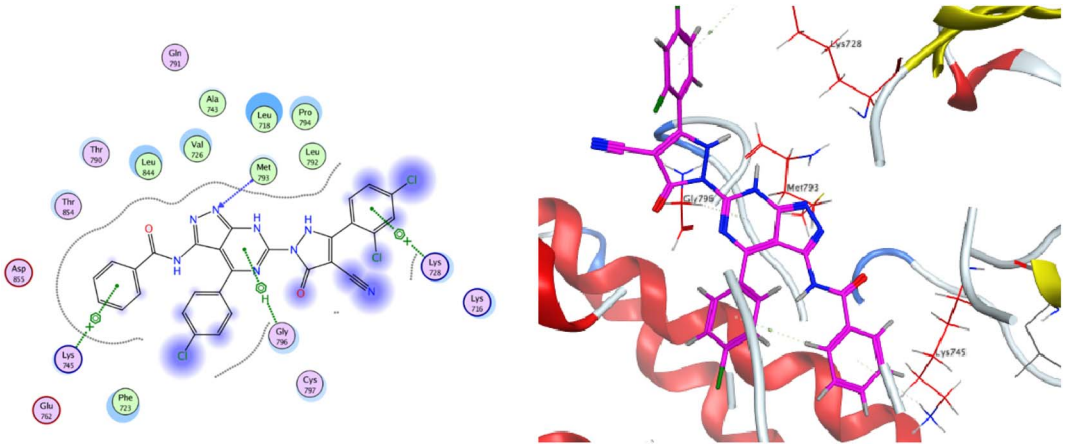

Fig. 12 2D and 3D binding mode of compound **15** inside the binding pocket of EGFR.

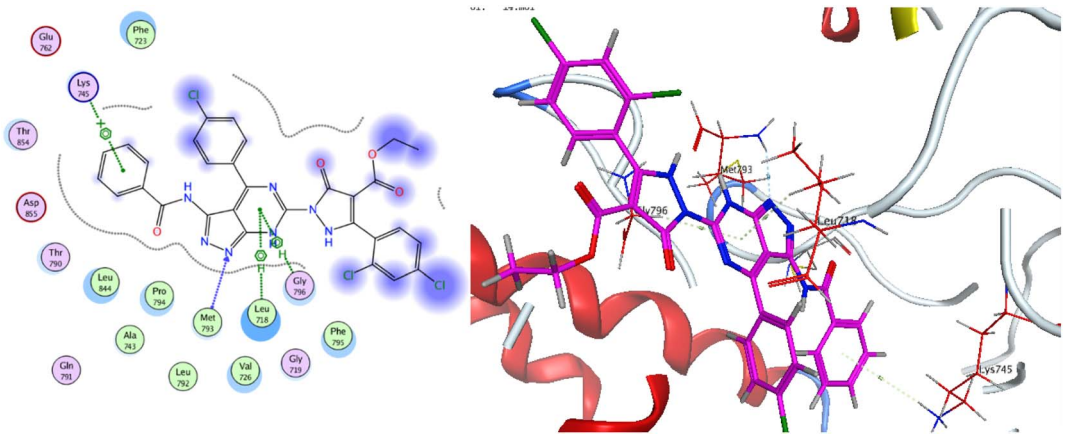

Fig. 13 2D and 3D binding mode of compound **16** inside the binding pocket of EGFR.

As for the newly designed pyrazolo[3,4-*d*]pyrimidine analogue **16**, the key amino acid residue Met793 interacted *via* a hydrogen bond with the nitrogen atom of the pyrazole ring. The binding mode of compound **16** presented three other essential binding interactions with the binding site of EGFR-TK. The pyrimidine ring formed two hydrophobic interactions with the key residues Leu718 and Gly796. Additionally, the terminal phenyl ring showed another arene interaction with Lys745. As a summary, it is noticeable that the pyrazolo[3,4-*d*] pyrimidine moiety of the target compounds oriented into the adenine binding site, forming an essential binding interaction with the key residue Gly796. The aryl ring linker to the amide linker and the substituted phenyl rings occupied hydrophobic tail and head, forming additional hydrophobic interactions with a number of amino acid residues, Fig. 13.

2.3.8. *In silico* ADMET studies. PKCSM online software (**https://biosig.lab.uq.edu.au/pkcsm/**) was used to estimate the physiochemical properties, and toxicity profile of compounds **15**, and **16**.[42]

The results showed that both compounds had considerable oral absorption values. However, derivative **16** showed better water solubility value. The study revealed that both compounds showed high cellular permeability, particularly for intestinal cells (89.689%, and 83.764%, respectively) (Table 4).

Compound **16** showed the higher BBB permeability and unbound fraction than its analog, in accordance to distribution predication. Also, the parameters related to metabolism and excretion did not exhibit considerable variations among the examined derivatives. Moreover, the toxicological properties of compounds **15** and **16** were examined. The tested analogues showed no toxicity to AMES, and they showed minimum values for oral rat acute toxicity (LD_{50}) and *Tetrahymena pyriformis* toxicity test. As for hERG I inhibition, both compounds predicted didn't inhibit hERG I enzyme but they inhibit hERG II which may help in decreasing side effects of heart including ventricular arrhythmia. These results represented might predict that both compounds **15** and **16** could be safe for human use.

2.4. Toxicological study

Initially, the doses 55, 90 and 100 mg kg^{-1} of compound **16** does not produce any significant effect on the animals. However, at the doses 1000 mg kg^{-1}, the rats showed the abdominal muscle contractions and ataxia signs after intrapretonial injection.

Table 4 ADMET predictions for the compounds **15**, and **16**

Property	Model name	Unit	**15**	**16**
Absorption	Water solubility	Numeric (log mol L^{-1})	−3.003	−2.902
	Caco2 permeability	Numeric (log Papp in 10^{-6} cm s^{-1})	0.632	0
	Intestinal absorption (human)	Numeric (% absorbed)	89.689	83.764
	P-glycoprotein substrate	Categorical (yes/no)	Yes	Yes
	P-glycoprotein I inhibitor	Categorical (yes/no)	Yes	Yes
	P-glycoprotein II inhibitor	Categorical (yes/no)	Yes	Yes
Distribution	Volume of distribution (human)	Numeric (log L kg^{-1})	−1.133	−0.169
	Fraction unbound (human)	Numeric (Fu)	0.049	0.099
	BBB permeability	Numeric (log BB)	−0.2.833	−0.2602
	CNS permeability	Numeric (log PS)	−2.428	−3.529
Metabolism	CYP2D6 substrate	Categorical (yes/no)	Yes	No
	CYP3A4 substrate	Categorical (yes/no)	Yes	Yes
	CYP1A2 inhibitor	Categorical (yes/no)	No	No
	CYP2C19 inhibitor	Categorical (yes/no)	Yes	No
	CYP2C9 inhibitor	Categorical (yes/no)	No	Yes
	CYP2D6 inhibitor	Categorical (yes/no)	No	No
	CYP3A4 inhibitor	Categorical (yes/no)	Yes	No
Excretion	Total clearance	Numeric (log ml min^{-1} kg^{-1})	0.055	0.131
	Renal OCT2 substrate	Categorical (yes/no)	No	No
Toxicity	AMES toxicity	Categorical (yes/no)	No	No
	Max. tolerated dose (human)	Numeric (log mg kg^{-1} per day)	0.626	0.642
	hERG I inhibitor	Categorical (yes/no)	No	No
	hERG II inhibitor	Categorical (yes/no)	Yes	Yes
	Oral rat acute toxicity (LD_{50})	Numeric (mol kg^{-1})	2.836	2.507
	Oral rat chronic toxicity (LOAEL)	Numeric (log mg kg^{-1}_bw per day)	4.144	3.314
	Hepatotoxicity	Categorical (yes/no)	Yes	No
	Skin sensitisation	Categorical (yes/no)	No	No
	T. pyriformis toxicity	Numeric (log ug L^{-1})	0.285	0.285
	Minnow toxicity	Numeric (log mM)	1.932	−0.635

Then, the animals showed labored breathing, gasping and finally death within 7 days. The percentage of animals that died at each dose was then transformed to probit using Finney's method. LD_{50} of compound **16** after intraperitoneal injection in rats determined in the present study was 100.3 mg kg^{-1}.

3. Conclusion

Four series of pyrazolo[3,4-*d*]pyrimidine were designed, synthesized as anti-proliferative agents exhibited potent anti-proliferative activity and apoptosis inducers in tumor cells. Two candidates exhibited significant broad spectrum anti-cancer activity in NCI 5-log dose screening against different cancer cell panel with GI_{50} values ranging from 2.53 to 9.63 μM, especially on leukemia, renal, melanoma and breast cancer cell lines. Accordingly, compound **16a** was chosen to further investigate the potential underlying mechanisms that induced cancer cell death. It was found that it has the ability to induce cell cycle arrest with concurrent increase in G1 and S population as well as increase the apoptotic cell population in time dependent manner. Moreover, the most significant anti-proliferative derivatives were evaluated for their EGFR inhibitory activity, that revealed the significant inhibition of the candidate **(4)** or cyano pyrazole derivative and its ethyl ester analogue (**15** and **16**) with IC_{50} of 0.054, 0.135 and 0.034 μM respectively. Finally, molecular docking study of the active compounds in EGFR kinase active site revealed their ability to form the essential H bond interactions with Met793, Gly796 and Lys745 key residues in the EGFR active site.

4. Experimental

4.1. Chemistry

An uncorrected Griffin and George melting-point equipment was used to calculate all melting points (Griffin & George Ltd., Wembley, Middlesex, UK). The purity of the chemicals produced was controlled using aluminum sheet silica gel F254 (Merck) thin layer chromatography (TLC). IR-spectra were acquired using the KBr wafer technique on a Pye Unicam SP1200 spectrophotometer (Pye Unicam Ltd., Cambridge, UK). The ^{1}H-NMR spectra were obtained using a Bruker Avance (III) with a Varian-Gemini 400 MHz and an internal standard of Tetramethyl silane (chemical shifts in scale ppm), while the ^{13}C-NMR spectra were obtained using a Bruker Avance (III) with a Varian-Gemini 400 MHz and an internal standard of Tetramethyl silane (chemical shifts in scale ppm). In deuterated Dimethylsulphoxide, TMS was utilized as an internal standard (DMSO-d_6). Elemental investigations were conducted out using a PerkinElmer 2400 CHN elemental analyzer at the Microanalytical Unit, Faculty of Science, Ain Shams University, and good analytical data (0.4) were obtained for all chemicals.

4.1.1. *N*-(4-(4-Chlorophenyl)-6-thioxo-6,7-dihydro-5*H*-pyrazolo[3,4-*d*]pyrimidin-3-yl)benzamide (2). Method (I): A solution of arylidene derivative **1** (1.6 g, 5 mmol) and thiourea

(0.38 g, 5 mmol) in absolute ethanol (10 mL) with base catalyst sodium ethoxide was refluxed for 3 h. The reaction mixture was followed by TLC. The precipitated product was filtered off and recrystallized from dioxane as (2.5 g, 67%).

Method (II): A mixture of arylidene derivative **1** (1.6 g, 5 mmol) and thiourea (0.38 g, 5 mmol) with base catalytic amount of sodium ethoxide was fused for 50 min at 180–185 °C in sand-bath. The reaction mixture was followed by TLC. The formed product was washed with boiling dioxane as (3.35 g, 88%). (Identity M.P., TLC, and IR).

Gold crystals; M.P. > 300 °C; IR (KBr) (υ_{max}, cm^{-1}): 3197 (NH_{br}), 3099, 3057 (CH aromatic), 1681 (C=O_{amide}), 1656 (C=N). ^{1}H-NMR (400 MHz, DMSO-d_6) δ_{ppm}: 6.75–6.76 (m, 5H, ArH), 7.69 (d, J = 3.44 Hz, 2H, $ArH_{p\text{-chloro}}$), 8.03 (d, J = 3.45 Hz, 2H, $ArH_{p\text{-chloro}}$), 11.46 (br s, 1H, NHCSNH, exchangeable with D_2O), 11.86 (br s, 1H, NHCSNH, exchangeable with D_2O), 12.40 (br s, 1H, PhCONH, exchangeable with D_2O). ^{13}C-NMR (100 MHz, DMSO-d_6) δ_{ppm}: 90.19, 112.88, 117.58, 124.37, 145.94, 146.48 (2C), 148.01 (2C), 150.07, 156.08, 156.79, 159.63, 170.94, 170.8, 171.55, 173.70, 187.64. Anal. Calcd for $C_{18}H_{12}ClN_5OS$ (381.84)%: C, 56.62; H, 3.17; N, 18.34; found: C, 56.64; H, 3.20; N, 18.31.

4.1.2. *N*-(4-(4-Chlorophenyl)-8-oxo-7,8-dihydropyrazolo[4,3-*e*]thiazolo[3,2-*a*]pyrimidin-3-yl)benzamide (3). Method (I): A solution of compound **2** (1.9 g, 5 mmol) was heated under reflux for 5 h in glacial acetic acid (15 mL) and chloroacetic acid (0.47 g, 5 mmol) and/or ethyl chloroacetate (0.61 mL, 5 mmol) with catalytic amount of sodium acetate anhydrous. After cooling, the reaction mixture was poured over crushed ice. To get **3**, the produced precipitate was filtered, dried, and recrystallized from ethanol/dioxane [3 : 1] as (2.69 g, 64%).

Method (II): A mixture of pyrazolo[3,4-*d*]pyrimidin **2** (1.9 g, 5 mmol) and chloroacetic acid (0.47 g, 5 mmol) and/or ethyl chloroacetate (0.61 mL, 5 mmol) with catalytic amount of sodium acetate anhydrous was fused for 75 min at 180–185 °C in sand-bath. TLC was used to monitor the reaction's progress. The formed product was washed with boiling ethanol as (3.32 g, 79%). (Identity M.P., TLC, and IR).

Red crystals; M.P. 284–286 °C; IR (KBr) (υ_{max}, cm^{-1}): 3270, 3129 (NH), 3091, 3006 (CH aromatic), 2962, 2924 (CH aliphatic), 1724 (C=O_{ketone}), 1698 (C=O_{amide}), 1650, 1618 (C=N). ^{1}H-NMR (400 MHz, DMSO-d_6) δ_{ppm}: 3.94 (s, 2H, CH_2), 6.67–6.71 (m, 2H, ArH), 7.11–7.19 (m, 2H, ArH), 7.95–8.00 (m, 3H, ArH), 8.01–8.3 (m, 2H, ArH), 12.91 (br s, 1H, PhCONH, exchangeable with D_2O). ^{13}C-NMR (100 MHz, DMSO-d_6) δ_{ppm}: 22.83, 116.04, 117.41, 120.44, 123.33, 123.69, 126.08, 128.56, 129.98, 131.66, 134.43, 140.38, 152.45, 158.87 (2C), 159.51 (2C), 166.93, 168.85, 169.66. Anal. Calcd for $C_{20}H_{12}ClN_5O_2S$ (421.86)%: C, 56.94; H, 2.87; N, 16.60; found: C, 56.64; H, 3.20; N, 18.31.

4.1.3. (*E*,*Z*)-*N*-(4-(4-Chlorophenyl)-7-(furan-2-ylmethylene)-8-oxo-7,8-dihydropyrazolo[4,3-*e*]thiazolo[3,2-*a*]pyrimidin-3-yl) benzamide (4). Method (I): A solution of pyrimidinethiol derivative **2** (1.9 g, 5 mmol), chloroacetic acid and furfural (0.48 mL, 5 mmol) in glacial acetic acid (15 mL) with a catalytic amount of morphline was refluxed for 5 h. The compound **4** was produced by filtering the heated product and washed it from hot acetic acid as (4.1 g, 92%).

Method (II): An ethanolic solution of compound **3** (2.1 g, 5 mmol) and furfural (0.48 mL, 5 mmol) with a catalytic amount of piperidine was refluxed for 3 h. TLC was used to monitor the reaction's progress. The compound **4** was produced by filtering the heated product and washed it from hot ethanol as (2.8 g, 63%).

Method (III): A mixture of compound **3** (2.1 g, 5 mmol) and furfural (0.48 mL, 5 mmol) with a catalytic amount of piperidine was fused under free solvent for 3 h. TLC was used to monitor the reaction's progress. The compound **4** was washed with boiling ethanol as (3.0 g, 84%).

Orange crystals; M.P. > 300 °C; IR (KBr) (υ_{max}, cm^{-1}): 3204, 3165 (NH), 3065, 3006 (CH aromatic), 1656 br (2C = O_{amide}). ^{1}H-NMR (400 MHz, DMSO-d_6) δ_{ppm}: 5.86 (s, 1H, =$CH_{olefinic}$), 7.35–7.37 (m, 2H, ArH), 7.52–7.56 (m, 3H, ArH), 7.67 (t, J = 7.99 Hz, 1H, ArH), 7.97–7.99 (m, 3H, ArH), 8.17–8.19 (m, 3H, ArH), 12.41 (br s, 1H, PhCONH, exchangeable with D_2O). Anal. Calcd for $C_{25}H_{14}ClN_5O_3S$ (499.93)%: C, 60.06; H, 2.82; N, 14.01; found: C, 60.09; H, 2.79; N, 14.05.

4.1.4. Ethyl 2-((3-benzamido-4-(4-chlorophenyl)-7*H*-pyrazolo[3,4-*d*]pyrimidin-6-yl)thio)acetate (5). A solution of pyrimidinethiol derivative **2** (1.9 g, 5 mmol) in dry acetone and ethyl chloroacetate (0.61 mL, 5 mmol) with dry potassium carbonate as a base catalysis was stirred at room temperature for 2 h. TLC was used to monitor the reaction's progress. The reaction mixture was acidified by diluted hydrochloric acid and crushed ice, the deposited solid was filtrated off and recrystallized from Ethanol/Dioxane [3 : 1] giving the pure compound **5** as yellow crystals (2.43 g, 53%); M.P. 188–190 °C; IR (KBr) (υ_{max}, cm^{-1}): 3308, 3160 (NH), 3061, 3002 (CH aromatic), 2930 (CH aliphatic), 1717 (C=O_{ester}), 1661 (C=O_{amide}), 1600 (C=N). ^{1}H-NMR (400 MHz, DMSO-d_6) δ_{ppm}: 2.06 (t, J = 8.25 Hz, 3H, CH_2CH_3), 4.35–4.44 (m, 2H, CH_2CH_3), 5.44 (s, 2H, SCH_2COOEt), 7.03–7.05 (m, 2H, ArH), 7.34–7.38 (m, 2H, ArH), 7.56–7.64 (m, 5H, ArH), 11.28 (br s, 1H, $NHSCH_2$, exchangeable with D_2O), 12.40 (br s, 1H, PhCONH, exchangeable with D_2O). ^{13}C-NMR (100 MHz, DMSO-d_6) δ_{ppm}: 21, 23, 55, 112, 114 (2C), 118, 127 (2C), 128, 129 (2C), 137, 141, 146, 152, 159, 166 (2C), 168 (2C), 174. Anal. Calcd for $C_{22}H_{18}ClN_5O_3S$ (467.93)%: C, 56.47; H, 3.88; N, 14.97; found: C, 56.45; H, 3.91; N, 14.75.

4.1.5. *N*-(4-(4-Chlorophenyl)-6-(methylthio)-7*H*-pyrazolo [3,4-*d*]pyrimidin-3-yl)benzamide (6). A solution of pyrimidinethiol derivative **2** (1.9 g, 5 mmol) and methyl iodide (0.71 mL, 5 mmol) with KOH (0.5 g, 10 mmol) in dry *N*,*N*-dimethylformamide (DMF) (10 mL) was stirred at 60 °C for 2.5 h. TLC was used to monitor the reaction's progress. The reaction mixture was acidified by cold diluted hydrochloric acid, the deposited solid was filtrated off and recrystallized from dry dioxane giving the pure compound **6** as orange crystals (3.47 g, 89%); M.P. 268–270 °C; IR (KBr) (υ_{max}, cm^{-1}): 3191 br (NH), 3057, 3002 (CH aromatic), 1680 (C=O_{amide}), 1656 (C=N). ^{1}H-NMR (400 MHz, DMSO-d_6) δ_{ppm}: 3.57 (s, 3H, SCH_3), 6.77–6.78 (m, 3H, ArH), 7.79–7.80 (m, 2H, ArH), 8.04–8.05 (m, 4H, ArH), 11.78 (br s, 1H, $NHSCH_3$, exchangeable with D_2O), 13.63 (br s, 1H, PhCONH, exchangeable with D_2O). ^{13}C-NMR (100 MHz, DMSO-d_6) δ_{ppm}: 15, 113, 116, 121, 124, 128 (2C), 131 (2C), 133 (2C), 141, 144 (2C), 145, 148 (2C), 167, 168. Anal. Calcd for

$C_{19}H_{14}ClN_5OS$ (395.87)%: C, 57.65; H, 3.56; N, 17.69; found: C, 57.68; H, 3.54; N, 17.72.

4.1.6. *N*-(4-(4-Chlorophenyl)-6-hydrazineyl-7*H*-pyrazolo [3,4-*d*]pyrimidin-3-yl)benzamide (7). Method (I): An ethanolic solution of compound **2** (1.9 g, 5 mmol) and hydrazine hydrate (0.5 mL, 10 mmol) was refluxed for 4 h. TLC was used to monitor the reaction's progress. The compound **7** was produced by filtering the heated product and washed it from boiling ethanol as (2.9 g, 78%).

Method (II): An ethanolic solution of compound **6** (1.95 g, 5 mmol) and hydrazine hydrate (0.5 mL, 10 mmol) was refluxed for 2.5 h. TLC was used to monitor the reaction's progress. The compound **7** was produced by filtering the heated product and washed it from boiling ethanol as (3.5 g, 92%).

Gray crystals; M.P. > 300 °C; IR (KBr) (υ_{max}, cm^{-1}): 3424, 3309 (NH_2), 3224, 3154 (NH), 3063 (CH aromatic), 1680 (C=O_{amide}), 1604 (C=N). ^{1}H-NMR (400 MHz, DMSO-d_6) δ_{ppm}: 6.75–6.76 (m, 3H, ArH), 7.27 (br s, 2H, $NHNH_2$, exchangeable with D_2O), 7.69–7.0 (m, 3H, ArH), 7.78 (br s, 1H, $NHCNHNH_2$, exchangeable with D_2O), 8.03–8.05 (m, 3H, ArH), 12.85 (br s, 1H, $NHNH_2$, exchangeable with D_2O), 13.69 (br s, 1H, PhCONH, exchangeable with D_2O). ^{13}C-NMR (100 MHz, DMSO-d_6) δ_{ppm}: 112.88 (2C), 117.61 (2C), 123.33, 123.69, 126.08, 131.66, 134.43, 140.38, 145.45, 148.04 (2C), 156.27, 159.08, 160.28, 169.81 (2C). Anal. Calcd for $C_{18}H_{14}ClN_7O$ (379.81)%: C, 56.92; H, 3.72; N, 25.82; found: C, 56.94; H, 3.75; N, 25.85.

4.1.7. *N*-(4-(4-Chlorophenyl)-8-thioxo-7,8-dihydro-6*H*-pyrazolo[4,3-*e*][1,2,4]triazolo[4,3-*a*]pyrimidin-3-yl)benzamide (8). A solution of hydrazine derivative **7** (1.9 g, 5 mmol) in dry pyridine and excess of carbon disulfide (3 mL) was heated in water-bath for 7 h. The deposited solid while heating was collected by filtration, dried and recrystallized from boiling dioxane to produce **8** as brown crystals; (3.7 g, 89%); M.P. > 300 °C; IR (KBr) (υ_{max}, cm^{-1}): 3180, 3164 (NH), 3051 (CH aromatic), 1660 (C=O_{amide}), 1626 (C=N). ^{1}H-NMR (400 MHz, DMSO-d_6) δ_{ppm}: 6.75–6.77 (m, 2H, ArH), 7.64–7.66 (m, 2H, ArH), 7.710–7.719 (m, 2H, ArH), 8.04–8.06 (m, 3H, ArH), 8.25 (br s, 1H, aCNHNH, exchangeable with D_2O), 11.44 (br s, 1H, aCNHNHCS, exchangeable with D_2O), 13.39 (br s, 1H, PhCONH, exchangeable with D_2O). ^{13}C-NMR (100 MHz, DMSO-d_6) δ_{ppm}: 112.94, 115.85, 117.75, 117.93, 129.74 (2C), 131.93 (2C), 132.04, 136.85 (2C), 146.12, 146.39 (2C), 148.22, 156.91, 159.10, 160.49, 171.52. Anal. Calcd for $C_{19}H_{12}ClN_7OS$ (421.86)%: C, 54.10; H, 2.87; N, 23.24; found: C, 54.07; H, 2.89; N, 23.27.

4.1.8. *N*-(4-(4-Chlorophenyl)-8-methyl-6*H*-pyrazolo[4,3-*e*][1,2,4]triazolo[4,3-*a*]pyrimidin-3-yl)benzamide (9). Hydrazine derivative **7** (1.9 g, 5 mmol) in glacial acetic acid was refluxed for 3 h. The deposited solid while heating was collected by filtration, dried and recrystallized from boiling acetic acid to produce **9** as orange crystals; (3.0 g, 77%); M.P. 280–282 °C; IR (KBr) (υ_{max}, cm^{-1}): 3167 (NH), 3087, 3028 (CH aromatic), 2972, 2917 (CH aliphatic), 1654 (C=O_{amide}). ^{1}H-NMR (400 MHz, DMSO-d_6) δ_{ppm}: 1.49 (s, 3H, CH_3), 7.32–7.34 (m, 3H, ArH), 7.68–7.77 (m, 2H, ArH), 7.94–7.95 (m, 2H, ArH), 8.04–8.09 (m, 2H, ArH), 11.43 (br s, 1H, aCNHNa, exchangeable with D_2O), 13.33 (br s, 1H, PhCONH, exchangeable with D_2O). ^{13}C-NMR (100 MHz, DMSO-d_6) δ_{ppm}: 22.64, 113.03 (2C), 116.20, 118.26 (2C), 125.48 (2C), 128.94 (2C), 134.88, 136.99 (2C), 137.88 (2C), 141.22, 148.49, 159.46, 167.95 (2C). Anal. Calcd for $C_{20}H_{14}ClN_7O$ (403.83) C, 59.49; H, 3.49; N, 24.28; found: C, 59.53; H, 3.51; N, 24.30.

4.1.9. *N*-(8-Benzyl-4-(4-chlorophenyl)-6*H*-pyrazolo[4,3-*e*][1,2,4]triazolo[4,3-*a*]pyrimidin-3-yl)benzamide (10). Hydrazine derivative **7** (1.9 g, 5 mmol) and phenyl acetic acid (0.69 g, 5 mmol) was fused in sand-bath at 180–185 °C for 1.5 h. TLC was used to monitor the reaction's progress. The formed product was washed with boiling ethanol as **10** yellow crystals; (4.2 g, 93%); M.P. 298–300 °C; IR (KBr) (υ_{max}, cm^{-1}): 3304, 3193 (NH), 3048 (CH aromatic), 1665 (C=O_{amide}), 1614 (C=N). ^{1}H-NMR (400 MHz, DMSO-d_6) δ_{ppm}: 4.64 (s, 2H, $PhCH_2Ca$), 7.56–7.64 (m, 6H, ArH), 7.81–7.86 (m, 3H, ArH), 8.10–8.17 (m, 3H, ArH), 11.97 (br s, 1H, aCNHNa, exchangeable with D_2O), 13.66 (br s, 1H, PhCONH, exchangeable with D_2O). ^{13}C-NMR (100 MHz, DMSO-d_6) δ_{ppm}: 21.13, 61.78, 68.28, 115.85 (2C), 116.66 (2C), 120.90, 123.02, 123.13, 125.59 (2C), 126.03 (2C), 127.77 (2C), 128.11, 128.46, 128.55, 129.89 (2C), 135.19, 146.74, 151.71, 170.62, 170.77. Anal. Calcd for $C_{26}H_{18}ClN_7O$ (479.93): C, 65.07; H, 3.78; N, 20.43; found: C, 65.09; H, 3.80; N, 20.40.

4.1.10. *N*-(4-(4-Chlorophenyl)-8-(phenylamino)-6*H*-pyrazolo[4,3-*e*][1,2,4]triazolo[4,3-*a*]pyrimidin-3-yl)benzamide (12). Method (I): A solution of hydrazine derivative **7** (1.9 g, 5 mmol) in dry pyridine with phenyl isothiocyanate (0.67 mL, 5 mmol) was refluxed for 15 h. The deposited solid while heating was collected by filtration, dried, and recrystallized from boiling dioxane to produce **12** as (2.78 g, 58%).

Method (II): A mixture of hydrazine derivative 6 (1.9 g, 5 mmol) and phenyl isothiocyanate (0.67 mL, 5 mmol) was fused for 2 h at 180–185 °C in sand-bath. TLC was used to monitor the reaction's progress. The formed product was washed with boiling dioxane to afford the pure compound **12** as (3.93 g, 82%). (Identity M.P., TLC, and IR).

Yellow crystals; M.P. > 300 °C; IR (KBr) (υ_{max}, cm^{-1}): 3240, 3197 (NH), 3060, 3035 (CH aromatic), 1686 (C=O_{amide}), 1605 (C=N). ^{1}H-NMR (400 MHz, DMSO-d_6) δ_{ppm}: 7.41–7.64 (m, 5H, ArH), 7.68–7.74 (m, 3H, ArH), 7.79–7.82 (m, 2H, ArH), 7.86–7.92 (m, 2H, ArH), 8.03–8.05 (m, 3H, ArH and −NHPh, exchangeable with D_2O), 13.56 (br s, 1H, aCNHNa, exchangeable with D_2O), 14.23 (br s, 1H, PhCONH, exchangeable with D_2O). ^{13}C-NMR (100 MHz, DMSO-d_6) δ_{ppm}: 124.27, 125.54, 127.48, 127.82, 128.11, 128.36, 129.21, 129.39, 130.04, 130.44, 131.08, 131.61, 132.14, 132.68, 133.12, 133.93, 136.45, 138.10, 139.00, 148.15, 151.51, 163.29, 166.36, 166.40, 173.87. Anal. Calcd for $C_{25}H_{17}ClN_8O$ (480.92) C, 62.44; H, 3.56; N, 23.30; found: C, 62.48; H, 3.59; N, 23.33.

4.1.11. General procedure for the synthesis of compounds (13a–c). Method (I): A mixture of compound **7** (1.9 g, 5 mmol) and the appropriate diketone derivatives namely; acetylacetone (0.50 mL, 5 mmol), ethyl acetoacetate (0.65 mL, 5 mmol) and/or benzoyl acetone (1.93 mL, 5 mmol) in absolute ethanol (15 mL) in the presence of a catalytic amount of triethylamine (TEA) was refluxed for 3 h. The precipitated crystals were filtered off and recrystallized from ethanol to afford compounds **13a–c** as (1.98 g, 45%), (2.24 g, 51%), and (1.2 g, 24%), respectively.

Method (II): A mixture of compound **7** (1.9 g, 5 mmol) and the appropriate diketone derivatives namely; acetylacetone

(0.50 mL, 5 mmol), ethyl acetoacetate (0.65 mL, 5 mmol) and/or benzoyl acetone (1.93 mL, 5 mmol) in the presence of a catalytic amount of triethylamine was fused under free solvent at 180–185 °C in sand-bath for one hour. The precipitated crystals were washed with boiling ethanol to afford the pure compounds **13a–c** as (2.46 g, 56%), (2.94 g, 67%), and (3.35 g, 67%), respectively.

4.1.12. *N*-(4-(4-Chlorophenyl)-6-(3,5-dimethyl-1*H*-pyrazol-1-yl)-7*H*-pyrazolo[3,4-*d*]pyrimidin-3-yl)benzamide (13a). Yellow crystals; M.P. > 300 °C; IR (KBr) (υ_{max}, cm^{-1}): 3150 (NH), 3002 (CH aromatic), 1679 (C=O_{amide}), 1637 (C=N). ^{1}H-NMR (400 MHz, DMSO-d_6) δ_{ppm}: 1.85 (s, 3H, CH_3), 1.89 (s, 3H, CH_3), 5.30 (s, 1H, =$CH_{olefinic}$), 6.67–6.70 (m, 3H, ArH), 7.11–7.18 (m, 2H, ArH), 7.62–7.63 (m, 4H, ArH), 7.98 (br s, 1H, aCNHCa, exchangeable with D_2O), 9.59 (br s, 1H, PhCONH, exchangeable with D_2O). Anal. Calcd for $C_{23}H_{18}ClN_7O$ (443.90): C, 62.23; H, 4.09; N, 22.09; found: C, 62.20; H, 4.12; N, 22.07.

4.1.13. *N*-(4-(4-Chlorophenyl)-6-(5-methyl-3-oxo-2,3-dihydro-1*H*-pyrazol-1-yl)-7*H*-pyrazolo[3,4-*d*]pyrimidin-3-yl) benzamide (13b). Gray crystals; M.P. > 300 °C; IR (KBr) (υ_{max}, cm^{-1}): 3331, 3178 (NH), 3088, 3073 (CH aromatic), 1694 br (C=O_{amide}), 1659, 1617 (C=N). ^{1}H-NMR (400 MHz, DMSO-d_6) δ_{ppm}: 2.11 (s, 3H, CH_3), 5.83 (s, 1H, =$CH_{olefinic}$), 7.53–7.57 (m, 3H, ArH), 7.65–7.71 (m, 3H, ArH), 7.98–8.02 (m, 3H, ArH), 11.28 (s br, 1H, aCNHCa, exchangeable with D_2O), 11.58 (br s, 1H, −NNHCO, exchangeable with D_2O), 12.40 (br s, 1H, PhCONH, exchangeable with D_2O). ^{13}C-NMR (100 MHz, DMSO-d_6) δ_{ppm}: 37.97, 68.28, 70.01, 120.90, 123.02, 123.13, 125.59 (2C), 126.03, 126.71, 127.77, 128.11, 128.46, 128.55, 129.80, 129.89, 135.19, 151.71, 152.70, 152.94, 161.70, 167.67. Anal. Calcd for $C_{22}H_{16}ClN_7O_2$ (445.87): C, 59.26; H, 3.62; N, 21.99; found: C, 59.28; H, 3.65; N, 22.03.

4.1.14. *N*-(4-(4-Chlorophenyl)-6-(3-methyl-5-phenyl-1*H*-pyrazol-1-yl)-7*H*-pyrazolo[3,4-*d*]pyrimidin-3-yl)benzamide (13c). Brown crystals; M.P. > 300 °C; IR (KBr) (υ_{max}, cm^{-1}): 3284, 3210 (NH), 3084, 3000 (CH aromatic), 1664 (C=O_{amide}), 1639 (C=N). ^{1}H-NMR (400 MHz, DMSO-d_6) δ_{ppm}: 1.96 (s, 3H, CH_3), 4.89 (s, 1H, =$CH_{olefinic}$), 7.18–7.22 (m, 2H, ArH), 7.36–7.39 (m, 2H, ArH), 7.61–7.65 (m, 6H, ArH), 7.99–8.01 (m, 2H, ArH), 8.64–8.66 (m, 2H, ArH), 9.05 (s br, 1H, aCNHCa, exchangeable with D_2O), 13.66 (br s, 1H, PhCONH, exchangeable with D_2O). ^{13}C-NMR (100 MHz, DMSO-d_6) δ_{ppm}: 21.01, 21.13, 115.85, 116.66, 120.90, 123.02, 123.13, 125, 126.03, 126.71, 127.77 (2C), 128.11 (2C), 128.46 (2C), 128.46 (2C), 128.55 (2C), 129.80 (2C), 129.89 (2C), 146.74, 151.71, 161.70, 167.67. Anal. Calcd for $C_{28}H_{20}ClN_7O$ (505.97): C, 66.47; H, 3.98; N, 19.38; found: C, 66.49; H, 4.01; N, 19.40.

4.1.15. General procedure for the synthesis of compounds (14–17). Method (I): A mixture of compound 7 (1.9 g, 5 mmol) with 2,4-dichlorobenzaldehyde (0.87 g, 5 mmol) and the appropriate active methylene derivatives namely; acetophenone (0.60 mL, 5 mmol), ethyl cyanoacetate (0.56 mL, 5 mmol), diethyl malonate (0.80 mL, 5 mmol) and/or malononitrile (0.33 mL, 5 mmol) in absolute ethanol (15 mL) in the presence of a catalytic amount of piperidine was refluxed for 3 h. TLC was used to monitor the reaction's progress. The precipitated crystals were filtered off and recrystallized from ethanol to afford compounds **14–17** as (3.9 g, 63%), (4.32 g, 72%), (3.57 g, 55%), and (4.86 g, 81%), respectively.

Method (II): A mixture of compound 7 (1.9 g, 5 mmol) with 2,4-dichlorobenzaldehyde (0.87 g, 5 mmol) and the appropriate active methylene derivatives namely; acetophenone (0.60 mL, 5 mmol), ethyl cyanoacetate (0.56 mL, 5 mmol), diethyl malonate (0.80 mL, 5 mmol) and/or malononitrile (0.33 mL, 5 mmol) in the presence of a catalytic amount of piperidine was fused under free solvent at 180–185 °C in sand-bath for 65–80 min. The precipitated crystals were washed with boiling ethanol to afford pure compounds **14–17** as (5.60 g, 89%), (5.22 g, 87%), (3.71 g, 58%), and (5.58 g, 93%), respectively.

4.1.16. *N*-(4-(4-Chlorophenyl)-6-(5-(2,4-dichlorophenyl)-3-phenyl-1*H*-pyrazol-1-yl)-7*H*-pyrazolo[3,4-*d*]pyrimidin-3-yl) benzamide (14). Yellow crystals; M.P. > 300 °C; IR (KBr) (υ_{max}, cm^{-1}): 3177 (NH), 3062 (CH aromatic), 1673 br (C=O_{amide}). ^{1}H-NMR (400 MHz, DMSO-d_6) δ_{ppm}: 5.35 (s, 1H, =$CH_{olefinic}$), 7.55–7.57 (m, 3H, ArH), 7.64–7.72 (m, 3H, ArH), 7.79–7.83 (m, 1H, ArH), 7.97–8.08 (m, 6H, ArH), 8.13–8.18 (m, 4H, ArH), 8.95 (s br, 1H, aCNHCa, exchangeable with D_2O), 14.14 (br s, 1H, PhCONH, exchangeable with D_2O). Anal. Calcd for $C_{33}H_{20}Cl_3N_7O$ (636.92): C, 62.23; H, 3.17; N, 15.39; found: C, 62.20; H, 3.19; N, 15.37.

4.1.17. *N*-(4-(4-Chlorophenyl)-6-(4-cyano-5-(2,4-dichlorophenyl)-3-oxo-2,3-dihydro-1*H*-pyrazol-1-yl)-7*H*-pyrazolo[3,4-*d*] pyrimidin-3-yl)benzamide (15). Brown crystals; M.P. 294–296 °C; IR (KBr) (υ_{max}, cm^{-1}): 3424, 3222 (NH), 3132 (CH aromatic), 2215 (C≡N), 1627 (C=O_{amide}). ^{1}H-NMR (400 MHz, DMSO-d_6) δ_{ppm}: 7.57–7.60 (m, 3H, ArH), 7.67–7.71 (m, 3H, ArH), 8.04–8.07 (m, 3H, ArH), 8.14–8.16 (m, 3H, ArH), 8.30 (s br, 1H, aCNHCa, exchangeable with D_2O), 10.90 (s br, 1H, −NNH − Ca, exchangeable with D_2O), 13.37 (br s, 1H, PhCONH, exchangeable with D_2O). Anal. Calcd for $C_{28}H_{15}Cl_3N_8O_2$ (601.83): C, 55.88; H, 2.51; N, 18.62; found: C, 55.85; H, 2.54; N, 18.59. Purity calculated is 69.69%.

4.1.18. Ethyl 1-(3-benzamido-4-(4-chlorophenyl)-7*H*-pyrazolo[3,4-*d*]pyrimidin-6-yl)-5-(2,4-dichlorophenyl)-3-oxo-2,3-dihydro-1*H*-pyrazole-4-carboxylate (16). Reddish brown crystals; M.P. 204–208 °C; IR (KBr) (υ_{max}, cm^{-1}): 3242, 3194 (NH), 3072 (CH aromatic), 2958, 2918 (CH aliphatic), 1715 (C=O_{ester}), 1666 (C=O_{amide}), 1606 (C=N). ^{1}H-NMR (400 MHz, DMSO-d_6) δ_{ppm}: 1.24 (t, J = 7.16 Hz, 3H, CH_2CH_3), 4.17 (q, J = 7.08 Hz, 2H, CH_2CH_3), 7.55–7.59 (m, 5H, ArH), 7.66–7.70 (m, 5H, ArH), 8.07–8.12 (m, 2H, ArH), 10.65 (s br, 1H, −NNH − Ca, exchangeable with D_2O), 12.89 (s br, 1H, −NNHCO, exchangeable with D_2O), 14.18 (br s, 1H, PhCONH, exchangeable with D_2O). Anal. Calcd for $C_{30}H_{20}Cl_3N_7O_4$ (648.89): C, 55.53; H, 3.11; N, 15.11; found: C, 55.58; H, 3.15; N, 15.13. Purity calculated is 90.92%.

4.1.19. *N*-(6-(3-Amino-4-cyano-5-(2,4-dichlorophenyl)-1*H*-pyrazol-1-yl)-4-(4-chlorophenyl)-7*H*-pyrazolo[3,4-*d*]pyrimidin-3-yl)benzamide (17). Yellow crystals; M.P. 252–254 °C; IR (KBr) (υ_{max}, cm^{-1}): 3210, 3149 (NH_2), 3129 br (NH), 3101 (CH aromatic), 2222 (C≡N), 1657 (C=O_{amide}), 1620 (C=N). ^{1}H-NMR (400 MHz, DMSO-d_6) δ_{ppm}: 6.88 (br s, 2H, NH_2, exchangeable with D_2O), 7.48–7.49 (m, 2H, CH_3), 7.52–7.56 (m, 4H, ArH), 7.65–7.69 (m, 2H, ArH), 7.97–7.99 (m, 4H, ArH), 8.20 (s br, 1H,

aCNHCa, exchangeable with D_2O), 11.82 (br s, 1H, PhCONH, exchangeable with D_2O). ^{13}C-NMR (100 MHz, DMSO-d_6) δ_{ppm}: 68.90, 100.05 (2C), 109.42, 116.06, 117.04 (2C), 120.52 (2C), 123.23 (2C), 123.86, 126.10 (2C), 128.60 (2C), 130.00 (2C), 131.15, 131.68, 134.65, 139.74, 140.38, 152.43, 159.67 (2C), 166.99, 169.64. Anal. Calcd for $C_{28}H_{16}Cl_3N_9O$ (600.85): C, 55.97; H, 2.68; N, 20.98; found: C, 56.00; H, 2.71; N, 21.02.

4.2. DFT studies

All calculations were carried out with Orca software.[43] All geometrical optimizations were carried out at the B3LYP/6-311+G(d,p) level.[44] The effect of were computed using UAHF (united atom topological model for Hartree–Fock) radii and a CPCM (conductor polarized continuum model).[45,46] All the calculated energies are the Gibbs free energies in toluene at 298 K.

4.3. Biological evaluation

4.3.1. Evaluation of cytotoxic activity against NCI 60 human cancer cell lines panel

4.3.1.1. Assay protocol. The human tumor cell lines of the cancer-screening panel were grown in RPMI 1640 medium containing 5% fetal bovine serum and 2 μM L-glutamine. For a typical screening experiment, cells are inoculated into 96 well microtiter plates in 100 mL at plating densities ranging from 5000 to 40 000 cells per well depending on the doubling time of individual cell lines. After cell inoculation, the microtiter plates are incubated at 37 °C, 5% CO_2, 95% air and 100% relative humidity for 24 h prior to addition of experimental drugs. After 24 h, two plates of each cell line are fixed *in situ* with TCA, to represent a measurement of the cell population for each cell line at the time of drug addition (Tz). Experimental drugs are dissolved in dimethyl sulfoxide at 400-fold the desired final maximum test concentration and stored frozen prior to use. At the time of drug addition, an aliquot of frozen concentrate is thawed and diluted to twice the desired final maximum test concentration with complete medium containing 50 mg mL^{-1} Gentamicin. Additional four, 10-fold or 1/2log serial dilutions are made to provide a total of five drug concentrations plus control. Aliquots of 100 mL of these different drug dilutions are added to the appropriate microtiter wells already containing 100 mL of medium, resulting in the required final drug concentrations. Following drug addition, the plates are incubated for an additional 48 h at 37 °C, 5% CO_2, 95% air, and 100% relative humidity. For adherent cells, the assay is terminated by the addition of cold TCA. Cells are fixed *in situ* by the gentle addition of 50 mL of cold 50% (w/v) TCA (final concentration, 10% TCA) and incubated for 60 min at 4 °C. The supernatant is discarded, and the plates are washed five times with tap water and air dried. Sulforhodamine B (SRB) solution (100 mL) at 0.4% (w/v) in 1% acetic acid is added to each well, and plates are incubated for 10 min at room temperature. After staining, unbound dye is removed by washing five times with 1% acetic acid and the plates are air dried. Bound stain is subsequently dissolved with 10 μM trizma base, and the absorbance is read on an automated plate reader at a wavelength of 515 nm. For suspension cells, the methodology is the same except that the assay is terminated by fixing settled cells at the bottom of the wells by gently adding 50 mL of 80% TCA (final concentration, 16% TCA).

4.3.1.2. Data analysis. Using the seven absorbance measurements [time zero, (Tz), control growth, (C), and test growth in the presence of drug at the five concentration levels (Ti)], the percentage growth is calculated at each of the drug concentrations levels. Percentage growth inhibition is calculated as: $[(Ti - Tz)/(C - Tz)] \times 100$ for concentrations for which Ti>/1/4Tz and $[(Ti - Tz)/Tz] \times 100$ for concentrations for which Ti < Tz.

Three dose response parameters are calculated for each experimental agent. Growth inhibition of 50% (GI_{50}) is calculated from $[(Ti - Tz)/(C - Tz)] \times 100 = 50$, which is the drug concentration resulting in a 50% reduction in the net protein increase (as measured by SRB staining) in control cells during the drug incubation. The drug concentration resulting in total growth inhibition (TGI) is calculated from Ti 1/4 Tz. The LC_{50} (concentration of drug resulting in a 50% reduction in the measured protein at the end of the drug treatment as compared to that at the beginning) indicating a net loss of cells following treatment is calculated from $[(Ti - Tz)/Tz] \times 100 = -50$. Values are calculated for each of these three parameters if the level of activity is reached; however, if the effect is not reached or is exceeded, the value for that parameter is expressed as greater or less than the maximum or minimum concentration tested.

4.3.2. *In vitro* EGFR tyrosine kinase activity.

EGFR served as the enzyme source and Poly (Glu, Tyr) sodium salt, (4 : 1, Glu : Tyr) (Sigma#P7244) served as the standardized substrate & Kinase-Glo Plus Luminescence kinase assay kit (Promega#V3772). The IC_{50} determination was carried out where quality control testing is routinely performed on each of the targets to insure compliance to acceptable standards. ^{33}P-ATP was purchased from PerkinElmer and ADP-Glo™ was purchased from Promega. All other materials were of standard laboratory grade.

4.3.2.1. Assay protocols. The EGFR tyrosine kinase activity was performed using Kinase-Glo Plus luminescence kinase assay kit (Promega). It measures kinase activity by quantitating the amount of ATP remaining in solution following a kinase reaction. The luminescent signal from the assay is correlated with the amount of ATP present and is inversely correlated with the amount of kinase activity. The compounds were diluted to 100 μM in 10% DMSO and 5 mL of the dilution was added to a 50 mL reaction so that the final concentration of DMSO is 1% in all of reactions. All of the enzymatic reactions were conducted at 30 °C for 40 min. The 50 μl reaction mixture contains 40 μM Tris, pH 7.4, 10 μM $MgCl_2$, 0.1 mg mL^{-1} BSA, 0.2 mg mL^{-1} Poly (Glu, Tyr) substrate, 10 μM ATP and EGFR. After the enzymatic reaction, 50 mL of Kinase-GloPlus Luminescence kinase assay solution (Promega) was added to each reaction and incubate the plate for 5 min at room temperature. Luminescence signal was measured using a BioTek Synergy 2 microplate reader. The protein kinase assays used to determine IC_{50} value were performed using ADP-GloTM assay kit from Promega which measures the generation of ADP by the protein kinase. Generation of ADP

by the protein kinase reaction leads to an increase in luminescence signal in the presence of ADP-GloTM assay kit. The assay was started by incubating the reaction mixture in a 96-well plate at 30 °C for 30 min. After the 30 min incubation period, the assay was terminated by the addition of 25 mL of ADP-GloTM Reagent (Promega). The 96 well plate was shaken and then incubated for 40 min at ambient temperature. 50 mL of Kinase detection reagent was added, the 96-well reaction plate was then read using the ADP-Glo Luminescences Protocol on a GloMax plate reader. Blank control was set up that included all the assay components except the addition of appropriate substrate (replace with equal volume of kinase assay buffer). The corrected activity for each protein kinase target was determined by removing the blank control value.

4.3.2.2. Data analysis. EGFR activity assays were performed in duplicate at each concentration. The luminescence data were analyzed using the computer software, Graphpad Prism. The difference between luminescence intensities in the absence of EGFR (Lu_t) and in the presence of EGFR (Lu_c) was defined as 100% activity ($Lu_t - Lu_c$). Using luminescence signal (Lu) in the presence of the compound, % activity was calculated as: % activity = $(Lu_t - Lu)/(Lu_t - Lu_c) \times 100\%$, where Lu = the luminescence intensity in the presence of the compound (all percent activities below zero were set to 0%). % Inhibition was calculated as: % inhibition = 100 (%) − % activity. IC_{50} determination for inhibitor against EGFR was estimated by generating a graph of log inhibitor *vs.* normalized response with variable using the Prism software.

4.3.3. Quantitative real time PCR for P-glycoprotein. The gene expression of P-gp was measured in MDA-MB-468 cells (1×10^5), which were exposed to compounds **15** and **16** (0.125, 0.250, 0.500, and 1.000 μM) for 72 h, using RT-PCR (Applied Biosystems 7500 Fast Real Time PCR System) according to the previous reported methods.

4.3.4. *In vitro* cytotoxicity of target compounds 15 and 16 in drug-resistant DOX/MDA-MB-468 cell line. We investigated the reversal DOX effect of the most active derivatives **15** and **16**, and assessed the IC_{50} of DOX/MDA-MB-4 according to MTT protocol assay.

4.3.5. Cell cycle analysis. MDA-MB-468 cells at a density of 4×10^6 cell/T 75 flask were exposed to compound **16** at its IC_{50} concentration for 24 and 48 h. The cells then were collected by trypsinization, washed with phosphate buffered saline (PBS), and fixed in ice-cold absolute alcohol. Thereafter, cells were stained, using Cycletest™ Plus DNA Reagent Kit (BD Biosciences, San Jose, CA), according to the manufacturer's instructions. Cell cycle distribution was determined using a FACS Calibur flow cytometer (BD Biosciences, San Jose, CA).

4.3.6. Measurement of apoptosis using annexin-V-FITC apoptosis detection kit. Apoptosis was determined by staining cells with Annexin V-fluorescein isothiocyanate (FITC) and counterstaining with propidium iodide (PI) using the Annexin V-FITC/PI apoptosis detection kit (BD PharMingen, San Diego, CA, USA) according to the manufacturer's instructions. Briefly, 4×10^6 cell/T 75 flask were exposed to compound **16** at its IC_{50} concentration for 24 and 48 h. The cells then were collected by trypsinization and 0.5×10^6 cells were washed twice with phosphate-buffered saline (PBS) and stained with 5 μl Annexin V-FITC and 5 μl PI in 1× binding buffer (BD PharMingen) for 15 minutes at room temperature in the dark. Analyses were performed using FACS Calibur flow cytometer (BD Biosciences, San Jose, CA).

4.3.7. Docking studies. Coordinates for EFGR crystal structure was retrieved from the Protein Data Bank (PDB code: 4ZAU) and handled consequently with Molecular Operating Environment program (MOE)[47] Non-essential ions, water molecules and ligand were discarded. Bond orders, formal charges and explicit hydrogen atoms were added to the complex structure. Subsequently, the most appropriate protonation states and optimization of the H-bond network were performed with the MOE 'Protonate 3D' function at standard settings (T = 300 K, pH = 7.0, ionic strength I = 0.1 mol l^{-1}). Energy minimization of all molecules was then performed using the MMFF94x force field at a gradient of 0.01 RMSD (*i.e.* if the gradient falls below RMSD, the minimization terminates). The docking experiments were conducted three times to extract simple descriptive statistics (*e.g.*, mean and standard deviation). This docking approach was validated by successful pose-retrieval of the co-crystallized ligand (YY3) when docked into its corresponding binding site of the crystal structure.

4.4. Calculation of LD_{50}

Twenty-five healthy adult male Wistar rats (weighing about 200 ± 20 g) were obtained from Animal House in Nahda University, Beni Suef, Egypt. All the animals were allowed to acclimatize to the experimental conditions for a period of 7 days. All the rats were housed in polyacrylic cages, not more than three animals per cage and maintained under standard laboratory conditions (natural light/dark cycle, room temperature 22 ± 3 °C). The experimental protocol was approved by the Ethical Committee in the university. Rats were fasted for 18 h prior to dosing. Compound **16** was administered once orally to the rats, using 22-gauze oral feeding needle. The volume of the dose depends on the size and weight of the animals. In rodents it should not exceed 1 mL/100 g body weight. In this study, compound **16** was dissolved in 0.5 mL of DMSO. An approximate LD_{50} can be determined by the so-called "up and down" or the "staircase method" using two animals and increasing the doses of compound **16**. Five doses were chosen which were given orally to five groups of rats, five rats in each group, for the determination of LD_{50} of compound **16** from 0% mortality to 100% mortality. After 24 h, the numbers of deceased rats in each group were counted, and percentage of mortality was calculated using the graphical method of Miller and Tainter.

Ethical approval

All animal procedures were performed in accordance with the guidelines for care and use of Animal House of Nahda University and approved by committee of ethics of scientific research

on living organisms at Faculty of Pharmacy, Nahda University, Beni-Suef, Egypt under reference number NUB-018-023.

Conflicts of interest

The authors declare no conflict of interest.

References

1 A. Detsi, M. Majdalani, C. A. Kontogiorgis, D. Hadjipavlou-Litina and P. Kefalas, Natural and synthetic 2'-hydroxy-chalcones and aurones: synthesis, characterization and evaluation of the antioxidant and soybean lipoxygenase inhibitory activity, *Bioorg. Med. Chem.*, 2009, **17**, 8073–8085, DOI: 10.1016/j.bmc.2009.10.002.

2 P. Traxler and P. Furet, Strategies toward the design of novel and selective protein tyrosine kinase inhibitors, *Pharmacol. Ther.*, 1999, **82**, 195–206, DOI: 10.1016/S0163-7258(98)00044-8.

3 P. S. Sharma, R. Sharma and T. Tyagi, Receptor tyrosine kinase inhibitors as potent weapons in war against cancers, *Curr. Pharm. Des.*, 2009, **15**, 758–776, DOI: 10.2174/138161209787582219.

4 A. Ocana, R. Serrano, R. Calero and A. Pandiella, Novel tyrosine kinase inhibitors in the treatment of cancer, *Curr. Drug Targets*, 2009, **10**, 575–576, DOI: 10.2174/138945009788488378.

5 S. Vogel, M. Barbic, G. Jurgenliemk and J. Heilmann, Synthesis, cytotoxicity, anti-oxidative and anti-inflammatory activity of chalcones and influence of A-ring modifications on the pharmacological effect, *Eur. J. Med. Chem.*, 2010, **45**, 2206–2213, DOI: 10.1016/j.ejmech.2010.01.060.

6 D. G. Piotrowska, M. Cieslak, K. Krolewska and A. E. Wroblewski, Design, synthesis, and cytotoxicity of a new series of isoxazolidines derived from substituted chalcones, *Eur. J. Med. Chem.*, 2011, **46**, 1382–1389, DOI: 10.1016/j.ejmech.2011.01.067.

7 S. Shenvi, K. Kumar, K. S. Hatti, K. Rijesh, L. Diwakar and G. C. Reddy, Synthesis, anticancer and antioxidant activities of 2,4,5-trimethoxy chalcones and analogues from asaronaldehyde: structure activity relationship, *Eur. J. Med. Chem.*, 2013, **62**, 435–442, DOI: 10.1016/j.ejmech.2013.01.018.

8 J. H. Cheng, C. F. Hung, S. C. Yang, J. P. Wang, S. J. Won and C. N. Lin, Synthesis and cytotoxic, anti-inflammatory, and anti-oxidant activities of 2',5'-dialkoxylchalcones as cancer chemopreventive agents, *Bioorg. Med. Chem.*, 2008, **16**, 7270–7276, DOI: 10.1016/j.bmc.2008.06.031.

9 M. Cherry and D. H. Williams, Recent kinase, and kinase inhibitor X-ray structures: mechanisms of inhibition and selectivity insights, *Curr. Med. Chem.*, 2004, **11**, 663–673, DOI: 10.2174/0929867043455792.

10 J. Smith, Erlotinib: small-molecule targeted therapy in the treatment of non-small-cell lung cancer, *Clin. Ther.*, 2005, **27**, 1513–1534, DOI: 10.1016/j.clinthera.2005.10.014.

11 G. R. Simon, J. C. Ruckdeschel, C. Williams, A. Cantor, A. Chiappori, C. M. Rocha Lima, S. Antonia, E. Haura, H. Wagner, L. Robinson, E. Sommers, M. Alberts and G. Bepler, Gefitinib (ZD1839) in previously treated advanced non-small-cell lung cancer: experience from a single institution, *Moffitt Cancer Center*, 2003, **10**, 388–395, DOI: 10.1177/107327480301000506.

12 A. J. Tevaarwerk and J. M. Kolesar, Lapatinib: a small-molecule inhibitor of epidermal growth factor receptor and human epidermal growth factor receptor-2 tyrosine kinases used in the treatment of breast cancer, *Clin. Ther.*, 2009, **31**(Pt 2), 2332–2348, DOI: 10.1016/j.clinthera.2009.11.029.

13 K. Bouchalova, M. Cizkova, K. Cwiertka, R. Trojanec, D. Friedecky and M. Hajduch, Lapatinib in breast cancer - the predictive significance of HER1 (EGFR), HER2, PTEN and PIK3CA genes and lapatinib plasma level assessment, *Biomed. Pap. Med. Fac. Univ. Palacky. Olomouc. Czech. Repub.*, 2010, **154**, 281–288, DOI: 10.5507/bp.2010.043.

14 P. Mahajan, N. Suri, R. Mehra, M. Gupta, A. Kumar and S. K. Singh, *Med. Chem. Res.*, 2017, **26**, 74, DOI: 10.1007/s00044-016-1728-2.

15 M. S. Abdelbaset, M. Abdel-Aziz, M. Ramadan, M. H. Abdelrahman, S. N. Abbas Bukhari, T. F. S. Ali and G. E. D. A. Abuo-Rahma, *Bioorg. Med. Chem.*, 2019, **27**, 1076, DOI: 10.1016/j.bmc.2019.

16 S. B. Yewale, S. B. Ganorkar, K. G. Baheti and R. U. Shelke, Novel 3-substituted-1-aryl-5- phenyl-6-anilinopyrazolo[3,4-d] pyrimidin-4-ones: docking, synthesis and pharmacological evaluation as a potential anti-inflammatory agents, *Bioorg. Med. Chem. Lett.*, 2012, **22**, 6616–6620, DOI: 10.1016/j.bmcl.2012.08.119.

17 M. Bakavoli, G. Bagherzadeh, M. Vaseghifar, A. Shiri, M. Pordel, M. Mashreghi, P. Pordeli and M. Araghi, Molecular iodine promoted synthesis of new pyrazolo[3,4-d]pyrimidine derivatives as potential antibacterial agents, *Eur. J. Med. Chem.*, 2010, **45**, 647–650, DOI: 10.1016/j.ejmech.2009.10.051.

18 B. S. Holla, M. Mahalinga, M. S. Karthikeyan, P. M. Akberali and N. S. Shetty, Synthesis of some novel pyrazolo[3,4-d] pyrimidine derivatives as potential antimicrobial agents, *Bioorg. Med. Chem.*, 2006, **14**, 2040–2047, DOI: 10.1016/j.bmc.2005.10.053.

19 J.-H. Chern, K.-S. Shia, T.-A. Hsu, C.-L. Tai, C.-C. Lee, Y.-C. Lee, C.-S. Chang, S.-N. Tseng and S.-R. Shih, Design, synthesis, and structure–activity relationships of pyrazolo [3,4-d]pyrimidines: a novel class of potent enterovirus inhibitors, *Bioorg. Med. Chem. Lett.*, 2004, **14**, 2519–2525, DOI: 10.1016/j.bmcl.2004.02.092.

20 A. Bazgir, M. M. Khanaposhtani and A. A. Soorki, One-pot synthesis and antibacterial activities of pyrazolo[4′,3′:5,6] pyrido[2,3-d]pyrimidine-dione derivatives, *Bioorg. Med. Chem. Lett.*, 2008, **18**, 5800–5803, DOI: 10.1016/j.bmcl.2008.09.057.

21 B. R. Neustadt, J. Hao, N. Lindo, W. J. Greenlee, A. W. Stamford, D. Tulshian, E. Ongini, J. Hunter, A. Monopoli, R. Bertorelli, C. Foster, L. Arik, J. Lachowicz, K. Ng and K.-I. Feng, Potent, selective, and orally active adenosine A2A receptor antagonists: arylpiperazine derivatives of pyrazolo[4,3-e]-1,2,4-triazolo[1,5-c]

pyrimidines, *Bioorg. Med. Chem. Lett.*, 2007, **17**, 1376–1380, DOI: 10.1016/j.bmcl.2006.11.083.

22 A. El-Mekabaty, Synthesis and Antioxidant Activity of Some New Heterocycles Incorporating the Pyrazolo[3,4-d] pyrimidin-4-one Moiety, *Chem. Heterocycl. Compd.*, 2015, **50**, 1698–1706, DOI: 10.1007/s10593-015-1640-6.

23 P. Gong, Y. F. Zhao and D. Wang, Synthesis and vasodilatory activities of new pyrazolo[3,4- d]pyrimidin-4-one derivatives, *Chin. Chem. Lett.*, 2002, **13**, 613–616.

24 K. W. Weitzel, J. M. Wickman, S. G. Augustin and J. G. Strom, Zaleplon: a pyrazolopyrimidine sedative-hypnotic agent for the treatment of insomnia, *Clin. Ther.*, 2018, **22**, 1254–1267, DOI: 10.1016/S0149-2918(00)83024-6.

25 B. D. Manning, Challenges and Opportunities in Defining the Essential Cancer Kinome, *Sci. Signaling*, 2009, **2**, pe15, DOI: 10.1126/scisignal.263pe15.

26 M. M. El-Enany, M. M. Kamel, O. M. Khalil and H. B. El-Nassan, Synthesis and antitumor activity of novel 6-aryl and 6-alkylpyrazolo[3,4-d]pyrimidin-4-one derivatives, *Eur. J. Med. Chem.*, 2010, **45**, 5286–5291, DOI: 10.1016/j.ejmech.2010.08.048.

27 X. J. Song, Y. Shao and X. G. Dong, Microwave-assisted synthesis of some novel fluorinated pyrazolo[3,4-d] pyrimidine derivatives containing 1,3,4-thiadiazole as potential antitumor agents, *Chin. Chem. Lett.*, 2011, **22**, 1036–1038, DOI: 10.1016/j.cclet.2011.05.012.

28 S. Gupta, L. M. Rodrigues, A. P. Esteves, A. M. F. Oliveira-Campos, M. S. J. Nascimento, N. Nazareth, H. Cidade, M. P. Neves, E. Fernandes, M. Pinto, N. M. F. S. A. Cerqueira and N. Brás, Synthesis of N-aryl-5-amino-4-cyanopyrazole derivatives as potent xanthine oxidase inhibitors, *Eur. J. Med. Chem.*, 2008, **43**, 771–780, DOI: 10.1016/j.ejmech.2007.06.002.

29 M. Devarakonda, R. Doonaboina, S. Vanga, J. Vemu, S. Boni and R. P. Mailavaram, Synthesis of novel 2-alkyl-4-substituted-amino-pyrazolo[3,4-d]pyrimidines as new leads for anti-bacterial and anti-cancer activity, *Med. Chem. Res.*, 2013, **22**, 1090–1101, DOI: 10.1007/s00044-012-0084-0.

30 P. Traxler, G. Bold, J. Frei, M. Lang, N. Lydon, H. Mett, E. Buchdunger, T. Meyer, M. Mueller and P. Furet, Use of a pharmacophore model for the design of EGF-R tyrosine kinase inhibitors: 4- (phenylamino) pyrazolo [3, 4-d] pyrimidines, *J. Med. Chem.*, 1997, **40**, 3601–3616, DOI: 10.1021/jm970124v.

31 A. A. Gaber, A. H. Bayoumi, A. M. El-Morsy, F. F. Sherbiny, A. B. M. Mehany and I. H. Eissa, Design, synthesis and anticancer evaluation of 1H-pyrazolo [3, 4-d] pyrimidine derivatives as potent EGFRWT and EGFRT790M inhibitors and apoptosis inducers, *Bioorg. Chem.*, 2018, **80**, 375–395, DOI: 10.1016/j.bioorg.2018.06.017.

32 V. K. Sharma, P. P. Nandekar, A. Sangamwar, H. P. Sánchez and S. M. Agarwal, Structure guided design and binding analysis of EGFR inhibiting analogues of erlotinib and AEE788 using ensemble docking, molecular dynamics and MM-GBSA, *RSC Adv.*, 2016, **6**, 65725–65735, DOI: 10.1039/C6RA08517B.

33 P. Traxler and P. Furet, Strategies toward the design of novel and selective protein tyrosine kinase inhibitors, *Pharmacol. Ther.*, 1999, **82**, 195–206, DOI: 10.1016/S0163-7258(98)00044-8.

34 S. R. Atta-Allah, A. M. AboulMagd and P. S. Farag, Design, microwave assisted synthesis, and molecular modeling study of some new 1,3,4-thiadiazole derivatives as potent anticancer agents and potential VEGFR-2 inhibitors, *Bioorg. Chem.*, 2021, **112**, 104923, DOI: 10.1016/j.bioorg.2021.104923.

35 P. S. Farag, M. M. Hemdan and A. A. El-Sayed, Nano nickel [1,2,4]-triazole-3-thiones complex: design, sonochemical synthesis, and antimicrobial evaluation, *J. Heterocycl. Chem.*, 2020, **57**, 3428–3441, DOI: 10.1002/jhet.4063.

36 M. H. Hekal, P. S. Farag, M. M. Hemdan and W. M. El-Sayed, New N-(1,3,4-thiadiazol-2-yl)furan-2-carboxamide derivatives as potential inhibitors of the VEGFR-2, *Bioorg. Chem.*, 2021, **115**, 105176, DOI: 10.1016/j.bioorg.2021.105176.

37 P. S. Farag, M. M. Hemdan and A. I. Hassaballah, The Reformatsky analogous reaction for the synthesis of novel β-thioxoesters via using aroyl isothiocyanates under solvent-free ball milling and conventional conditions, *RSC Adv.*, 2022, **12**, 10204, DOI: 10.1039/D2RA01154A.

38 P. S. Farag, A. M. AboulMagd, M. M. Hemdan and A. I. Hassaballah, Annulated pyrazole derivatives as a novel class of urokinase (uPA) inhibitors: green synthesis, anticancer activity, DNA-damage evaluation, and molecular modelling study, *Bioorg. Chem.*, 2023, **130**, 106231, DOI: 10.1016/j.bioorg.2022.106231.

39 T. Shaikh, A. Gosar and H. Sayyed, Nitrosamine Impurities in Drug Substances and Drug Products, *J. Adv. Pharm. Pract.*, 2020, **2**, 48–57, DOI: 10.5281/zenodo.3629095.

40 H. Akkaraju, R. Tatia, S. S. Mane, A. B. Khade and S. J. Dengale, A comprehensive review of sources of nitrosamine contamination of pharmaceutical substances and products, *Regul. Toxicol. Pharmacol.*, 2023, **139**, 105355, DOI: 10.1016/j.yrtph.2023.105355.

41 S. Pani, S. Mohapatra, A. Sahoo, B. Baral and P. R. Debata, Shifting of cell cycle arrest from the S-phase to G2/M phase and downregulation of EGFR expression by phytochemical combinations in HeLa cervical cancer cells, *J. Biochem. Mol. Toxicol.*, 2022, **36**, e22947, DOI: 10.1002/jbt.22947.

42 D. E. Pires, T. L. Blundell and D. B. Ascher, pkCSM: predicting small-molecule pharmacokinetic and toxicity properties using graph-based signatures, *J. Med. Chem.*, 2015, **58**(9), 4066–4072.

43 F. Neese, Software update: the ORCA program system, version 4.0, *Wiley Interdiscip. Rev.: Comput. Mol. Sci.*, 2017, **8**, e1327, DOI: 10.1002/wcms.1327.

44 J. Antony and S. Grimme, Density functional theory including dispersion corrections for intermolecular interactions in a large benchmark set of biologically relevant molecules, *Phys. Chem. Chem. Phys.*, 2006, **8**, 5287–5293, DOI: 10.1039/B612585A.

45 V. Barone and M. Cossi, Quantum calculation of molecular energies and energy gradients in solution by a conductor

solvent model, *J. Phys. Chem.*, 1998, **102**, 1995–2001, DOI: 10.1021/jp9716997.

46 M. Cossi, N. Rega, G. Scalmani and V. Barone, Energies, structures, and electronic properties of molecules in solution with the C-PCM solvation model, *J. Comput. Chem.*, 2003, **24**, 669–681, DOI: 10.1002/jcc.10189.

47 *MOE*, Chemical Computing Group Inc., Montreal, https://www.chemcomp/com.